Summer 8-15-2014

Optical Resonators and Fiber Tapers as Transducers for Detection of Nanoparticles and Bio-Molecules

Huzeyfe Yilmaz
Washington University in St Louis

Washington University in St. Louis

School of Engineering and Applied Science

Department of Electrical and Systems Engineering

Thesis Examination Committee:
Lan Yang, Chair
Srikanth Singamaneni
Viktor Gruev

Optical Resonators and Fiber Tapers as Transducers for Detection of Nanoparticles and Bio-Molecules

by

Huzeyfe Yilmaz

A thesis presented to the School of Engineering and Applied Science
of Washington University in partial fulfillment of the
requirements for the degree of

Master of Science

August 2014
Saint Louis, Missouri

Contents

List of Tables

List of Figures

Acknowledgments

First of all I would like to thank my advisor Dr. Lan Yang for giving me the chance to work in Micro/Nano Photonics Lab, for her guidance, kindness and generous help throughout my Master of Science Thesis research. Then I would like to thank Dr. Srikanth Singamaneni and Dr. Victor Gruev for participating as committee members in my thesis and their valuable feedback. I would also like to thank Micro/Nano Photonics Lab members; Faraz Monifi, Jiangang Zhu, Bo Peng and He Huang for their help in the laboratory and for the discussions we had. For their endless love and support, I would like to thank my parents and my brother.

Huzeyfe Yilmaz

Washington University in Saint Louis
August 2014

ABSTRACT OF THE THESIS

Optical Resonators and Fiber Tapers as Transducers for Detection of Nanoparticles and Bio-Molecules

by

Huzeyfe Yilmaz

Master of Science in Electrical Engineering

Washington University in St. Louis, August 2014

Research Advisor: Professor Lan Yang

In recent years, detection of biological interactions on single molecule level has aspired many researchers to investigate several optical, chemical, electrical and mechanical sensing tools. Among these tools, toroidal optical resonators lead the way in detection of the smallest particle/molecule with real time measurements. In this work, bio-sensing capabilities of toroidal optical resonators are investigated. Bio-sensing is realized via measuring the analyte-antigen interaction while the antigen is immobilized through a novel functionalization method. Lately, detection of single nanoparticles using optical resonators have been accomplished however the need for cost-effective and practical transducers demands simpler tools. A tapered optical fiber is a suitable and efficient candidate as a practical tool. In this work, single nanoparticle detection measurements are performed in aqueous solutions and detection limit of fiber taper is investigated.

Chapter 1

Biosensing Using Microtoroid Optical Resonators

1.1 Label Free Sensing

1.1.1 Definition

The main goal of bio-sensing is to generate a concentration dependent electronic signal using a **physio-chemical transducer** associated with a **biological sensing element** to interact with the target probe which is a bio-molecule in the scope of this thesis [25]. Until recently direct detection of bio-molecules and real time measurements of bio-molecule dynamics was not possible. Instead, indirect measurements which required the probe to be labeled with a marker -such as a fluorescent dye- were routine procedures. Even though such measurements are useful for research purposes, health-care diagnostics and further fundamental research demands label-free sensing with an ultimate objective of detecting single molecules and molecular dynamics. Consequently, last decade has witnessed tremendous effort and achievement towards real time single molecule detection in label free sensing. A label free sensor is a mechanical, electrical or optical transducer with the ability to provide direct information about the bio-molecule or the probe in real time, ideally with single molecule sensitivity [11]. In order to detect a bio-molecule (target probe), the transducer has to react to a target probe property. Different transducers react to different properties of a probe. For example, electrical detection is via change in current, voltage or resistance using refractive index or other electrical properties of the target probe; optical detection is

via change in intensity, optical resonance frequency or interference using refractive index or electronic properties of the target probe; mechanical detection is via change in mechanical resonance frequency using the mass of the target probe, etc [9, 19, 3, 28, 29]. Certain properties of a specific target probe are more prominent than others therefore there is necessity for variety of detection techniques which offer a wide range of tools that are used for various target probes with sensitivity upheld as the essential and primary matter.

1.1.2 Sensitivity

In order to analyze the limits of a sensor the parameters affecting the sensitivity must be studied. Evidently, the smallest change that can be detected by a sensor determines its sensitivity. Therefore, the attribute which allows a detection signal to be measured from a transducer shall have a property to decide on how *good* a transducer is. For example an optical resonance is the attribute of an optical resonator (transducer) via which detection signal is obtained and the *goodness* of a resonance is defined by its **quality factor (Q)**. On the other hand, the *amount* of the exposure of a target probe property to the mechanism of a transducer will also affect the detection signal. Following the previous example, an optical resonator to be used as a transducer exploits the polarizability of the target probe via the evanescent resonant field intensity. Hence, with a larger evanescent field intensity the target probe will be more polarized and a larger sensing signal will be obtained. For an optical resonator smaller volumes for resonant fields result in higher intensities and **mode volume (V)** is the parameter responsible for the *amount* of target probe polarization. Note that, the target probe will be more polarized with a smaller mode volume.

1.1.3 Functionalization

By definition bio-sensing is made possible via biological sensing element - target probe interaction. Therefore, in the case of label free sensing functionalization of the transducer interface with ligands, receptors or complementary strands is necessary for immobilizing and detecting antibodies, carbohydrates, cells, drugs, or DNA-RNA strands [20]. Even though non-functional sensing methods such as non-specific particle/molecule trapping, size/mass sorting are existent, single molecule sensitivity demands more sophisticated methods which

makes immobilization of the target probe inevitable. Ordinarily, functionalization processes aim to obtain an efficient biological sensing element -which is to have maximum possible density of the sensing element on the transducer surface- but depending on the transducer's surface chemistry and fragility to chemical modification such a task becomes challenging. The transducer surface is in general inorganic and the functionalization process is primarily silanization. For their stability, silanized surfaces introduce restrictions to the sensing environment such as control over the pH, solvent, temperature and other parameters. Then, not only the scope of the biosensor is narrowed but also for the case of real world applications non-precise control of sensing environment conditions reduce the stability of the biological sensing element-transducer association not to mention the possible alterations in the target probe-sensing element affinity. Since the sensitivity of the transducer is limited by the number of available complementary agents on the transducer surface, sensitivity is also limited. Furthermore, when transport of molecules in extremely low concentrations is diffusion based unpractical measurements times are required for detection. Perhaps researchers may surmount such difficulties by performing long experiments however the validity of the data obtained from such experiments remains to be dubious. Finally, since the association of sensing element and the transducer requires chemical manipulation of the transducer interface, in general functionalization processes deteriorate the performance of the bio-sensor and single molecule detection vanishes from the reach of label free sensors. In this work a novel functionalization method is proposed with minimal chemical manipulation and no significant deterioration in sensing performance of the transducer within reasonable transport times using a microfluidic flow system.

1.1.4 Label Free Sensing Methods

As mentioned earlier, label free sensing is made possible by obtaining an electronic signal from the transducer as the bio-molecule -target probe- interacts with the biological sensing element. So far the interaction and performance of the transducer with the target probe is explained. As outlined above label free sensing demands different types of transducers and mechanisms. Primarily, transducers use mechanical, electrical or optical mechanisms. This section aims to provide a background in the recent developments in different label free sensing methods based on their aforementioned transducer mechanisms with a more focused

attention in optical sensors for the sake of this thesis.

Detection of proteins and DNA strands have been the prime target for electrical sensors using the change in electrical properties such as conductance or impedance. Electrical sensors based on nanowires or nantubes have recently proven to have high sensitivities. Moreover, recent developments in lithography techniques opens up the possibility of fabricating such devices in a fully integrated platform. For example, in a work reported by Zheng *et al.* [33] electrical detection and multiplexing of extremely diluted (0.9 pg/ml) serum solutions of prostate specific antigen and carcinoembryonic antigen using silicon nanowire sensor arrays have been demonstrated. Besides the praiseworthy sensitivity, arrays of silicon nanowire sensors provide false positive discrimination and multiplexing capabilities which augment applications to diagnosis and treatment of complex diseases.

Mechanical sensors on the other hand consistently use cantilevers for detection. In the case of a mechanical sensor, the transducer uses changes in the stress/strain profile or changes in the mechanical resonance frequency of the cantilever. In 2007, Burg *et al.* [3] have successfully weighed single bacterial cells with sub-femtogram resolution using suspended microchannel resonators. Making use of low resonator mass and relatively high quality factors such mechanical resonators have the possible use in direct detection of pathogens and sizing of colloidal particles in the future.

Optical sensors have a wider range of phenomena to base sensing their methods on such as interference, polarization, refractive index, absorption, luminescence, Raman scattering, light scattering, photo-acoustic effects and surface plasmons. At present there are various commercially available and commonly used optical biosensors such as Optical Grating-Coupled Waveguide biosensors (OWLS), Dual Polarization Interferometers (DPI), Surface Plasmon Resonance based biosensors (SPR), Wavelength Interrogated Optical Systems (WIOS) that use evanescent fields, Optical Immuno Assays (OIA)that use interference and Ellipsometers (ELM) that use reflection all of which enable researchers to understand biological interactions and help detect bio-molecules using different techniques. Optical bio-sensing techniques can be studied in three main categories:

- Reflection based techniques
- Interference based techniques
- Evanescent field techniques

Reflection based sensing is realized with a reflective surface (transducer) and functionalization of the surface with the complementary group (sensing element). Transducer signal is obtained by changes in the phase or the amplitude of the light reflecting from the surface and information about the thickness and the refractive index of the bio-molecule can be gathered. Reflection based sensing provides label free sensing with 1 ng sensitivity along with imaging possibility owing to its lateral resolution however requires very flat surfaces and the results are often model based since the refractive index and thickness values are determined by fitting parameters into equations defining the reflection coefficients.

Optical interference has a wide range of applications ranging from astronomy, spectroscopy and lasers to biological imaging and microscopy. Simply put, interference is two electromagnetic waves superimposed and carries information about phase difference between the two waves. In interference based optical biosensors optical thin films are used. Interference becomes very sensitive to the thickness of the thin film and when functionalized with the sensing element optical thin film attains the ability to immobilize and detect target probes via changes in the interference pattern. With recent developments optical immuno assays have become commercial systems for bacteria screening. However such systems only yield a monolayer detection sensitivity and single molecule sensitivity lies far ahead.

Evanescent field techniques rely on well known Snell's law for refraction of light from surfaces with different refractive indices. When the angle of incidence of the light beam is larger than

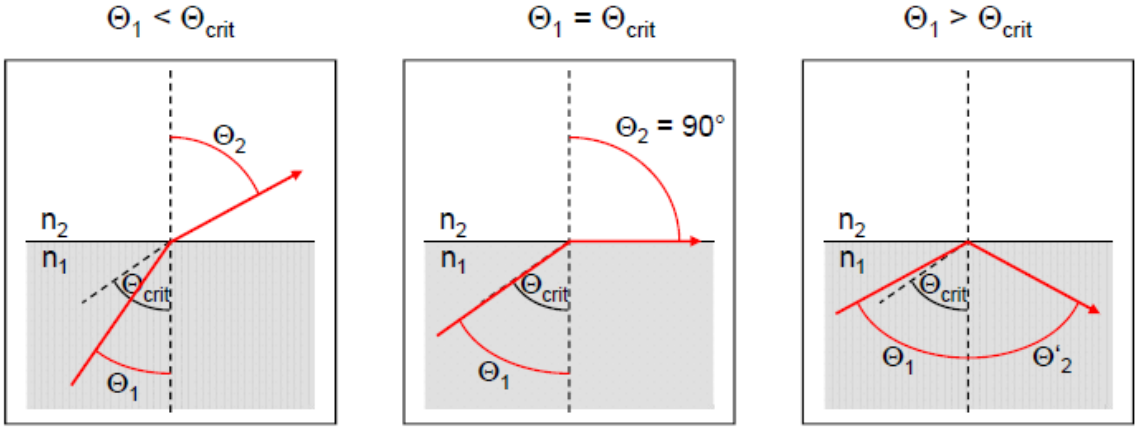

Figure 1.1: Refraction of light for different angles of incidence for $n_1 > n_2$. (Recall Snell's Law: $n_1 \sin\theta_1 = n_2 \sin\theta_2$.)

the critical angle, light beam undergoes total internal reflection. In this case a wave with

exponentially decaying intensity as a function of the distance from the surface is formed at the boundary between the two media with refractive indices n_1 and n_2. The surface of the medium with the smaller refractive index is functionalized with the biological sensing element and target probe bio-molecules binding to the surface induce changes in the evanescent field hence biosensing is accomplished. Surface Plasmon Resonance based biosensors (SPR) and Optical Grating-Coupled Waveguide biosensors (OWLS) use evanescent field principles for sensing. SPR biosensors offer 0.1 ng sensitivity however require noble metal surfaces where OWLS offer lower sensitivity (1 ng) but require waveguides with lithographically fabricated gratings. Recently, localized SPR biosensors (LSPR) have attracted immense attention due to greatly enhanced field intensities by confinement of the surface plasmon resonance in a nanoparticle. LSPRs demonstrate that sensitivity is dependent on the two parameters: Even with relatively low quality *quality factors* extremely low *mode volumes* make them valuable tools in the quest of single molecule detection. For instance McFarland *et al.* [17] have demonstrated detection of fewer than 60000 molecules forming a monolayer on individual Ag nanoparticles corresponding to zeptomolar sensitivity via localized surface plasmon resonances with real time measurements.

In addition to the evanescent field methods mentioned above, photonic crystal cavities have also been incorporated into biosensing platforms. Photonic crystal cavities also profit from highly localized fields with the possibility of building integrated biosensor devices. In 2009, Mandal *et al.* [16] have shown detection and multiplexing of interleukin 4,6 and 8 with a limit of 63 ag of total mass.

Cavity enhanced sensing is another biosensing technique that makes use of evanescent field principles. Biosensing using microtoroidal cavity enhancement constitutes the first part of this thesis and will be discussed in greater detail in the following section.

1.2 Cavity Enhanced Biosensing

1.2.1 Quality Factor and Mode Volume

Optical cavities (resonators) have been of interest since the invention of the laser. Analogous to electrical resonators optical cavities confine light at cavity morphology dependent resonance frequencies. The simplest of optical cavities is the Fabry-Perot cavity which consists

of two perfect parallel mirrors. Enhancement of light is achieved by reflection from the two mirrors many times with little loss. Further enhancement is obtained by confining light in

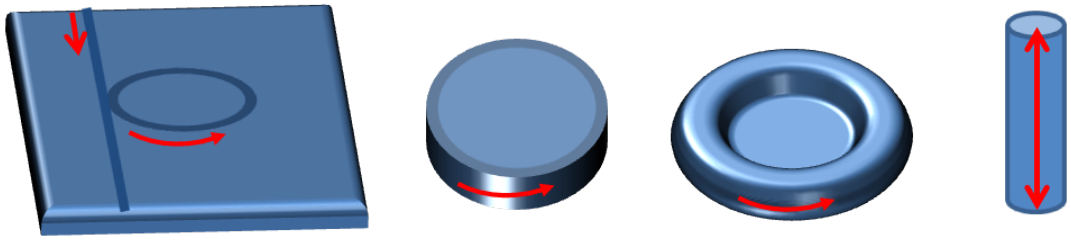

Figure 1.2: Light confinement in optical microcavities: Microring, microdisk, microtoroid and micropillar cavities.

much smaller volumes. When the wavelength of the confined light is comparable to the size of the cavity, such optical resonators are called microcavities. Microspheres, microrings, liquid core optical ring resonators (LCORR) and microtoroids make use of the spherical/circular symmetry and confine light via total internal reflection where micropillars rely on the Fabry-Perot principle.
The following parameters characterize an optical microcavity:

- Quality factor, a figure of merit for defining the lifetime (τ_0) of a photon in the microcavity
- Mode volume, the volume taken up by the confined light in the microcavity

Quality Factor The capability of an optical microcavity is primarily defined by the loss. The photon lifetime, τ_0, is directly related to the loss $1/\tau_0$ hence the quality factor, Q, is the most essential parameter in characterizing a microcavity. Therefore Q can be defined as the ratio of the *field energy stored in the cavity* and the *power dissipated by the cavity*. Then the cavity loss can also be expressed in terms of the quality factor. As a function of the cavity resonance frequency

$$Q = \frac{\lambda}{\Delta\lambda} = \omega\tau \tag{1.1}$$

where λ is the resonance wavelength, $\Delta\lambda$ is the linewidth of the resonance, ω is the resonance frequency ($\omega = 2\pi c/\lambda$) and τ is the loss in the cavity. Since there are several mechanisms responsible for loss in a cavity, these mechanisms are also responsible for the limitation of

the Q

$$\frac{1}{Q_{total}} = \frac{1}{Q_{material}} + \frac{1}{Q_{surface}} + \frac{1}{Q_{radiation}} + \frac{1}{Q_{coupling}} \tag{1.2}$$

where $1/Q_{material}$ is responsible for material losses, $1/Q_{surface}$ corresponds to losses due to surface imperfections, $1/Q_{radiation}$ is due to radiation losses in the cavity and losses due to input/output coupling is defined as $1/Q_{coupling}$. Aside from coupling losses, remaining loss mechanisms are intrinsic to the cavity and equation 1.2 can be simplified to

$$\frac{1}{Q_{total}} = \frac{1}{Q_{intrinsic}} + \frac{1}{Q_{coupling}} \tag{1.3}$$

Mode Volume As mentioned in the earlier sections mode volume has an important role for applications of optically resonant devices. Microcavities have the ability to confine light in very small physical volumes and to attain high Q factors, resulting in enhancement of the light intensity (hence the energy density) inside the cavity. Mode volume can be expressed as

$$V = \frac{\int \epsilon(\vec{r})|\vec{E}|^2 \mathrm{d}^3\vec{r}}{|\vec{E}_{max}|^2} \tag{1.4}$$

where $|\vec{E}|$ is the electric field in the cavity, $\epsilon(\vec{r}) = n^2(\vec{r})$ is the refractive index squared and V is the mode volume. Now the parameters for characterization of microcavities established, the following table shall help classify and compare optical microcavities for their biosensing capabilities. It is evident that microtoroids and microspheres make use of high quality fac-

Table 1.1: Mode volume and quality factor for different microcavities

Microcavity	**Mode Volume**	**Quality Factor**
Microring[15]	5	10^5 in air 10^5 in aqueous environment
Microtoroid[35]	10^2	10^8 in air 10^7 in aqueous environment
Microshpere[28, 8]	10^3	10^9 in air 10^6 in aqueous environment
LCORR[7]	10^2	10^5 in air 10^5 in aqueous environment
Photonic Crystal[5]	1	10^4 in air 10^4 in aqueous environment

tors where microrings, LCORR devices and photonic crystals use smaller mode volumes. In order to characterize the sensitivity of an optical resonance based biosensor Q/V can be used since higher quality factors with smaller mode volumes are desirable. In general, biosensing

requires use of the transducer in various solutions for the preservation of the target probe-sensing element affinity. Therefore the reduction of quality factor due to increased medium refractive index has to be taken into account. When the outside refractive index is increased radiation losses of an optical cavity increases which leads to a decrease in the quality factor. Drastic refractive index changes in the medium changes the entire morphology of the cavity since the refractive index of it is effectively modified $n_{eff} = n_{cavity}/n_{medium}$. In order to compensate the radiation losses a lower limit on the size of the resonator is then necessary which at the same time increases the mode volume. Even though smaller cavity sizes are attainable with photonic crystal cavities at the present they lack the quality factors necessary for single molecule detection. With the same token, comparison of microrings, LCORR devices and microtorids, puts microtoroids one step ahead in their sensing capabilities for taking steps towards single molecule sensing. However, it is paramount to note that microtoroids with their high quality factors and relatively small mode volumes also have their handicaps since these parameters also make them responsive to noise mechanisms, such as temperature fluctuations in the environment.

1.2.2 Cavity Enhanced Sensing Theory

This section aims to introduce the theory of sensing using optical microcavities. As mentioned in the previous sections, the sensitivity of microcavities is dependent essentially on the morphology of the resonance; mode volume and the quality factor. Electromagnetic wave equation needs to be solved in order to apprehend the optical resonance profile in a microcavity

$$\bigtriangledown^2\mathbf{E}(\mathbf{r}) - k^2\varepsilon(\mathbf{r})\mathbf{E}(\mathbf{r}) = 0 \tag{1.5}$$

Unfortunately closed form expressions of the solutions of equation 1.5 for the microtoroid geometry does not exist. Microtoroid geometry consists of a torus located around a disk through which the torus is supported by a pillar.

This geometry is defined by the major diameter D (principle diameter of the torus) and the minor diameter d (inner diameter of the torus) disregarding the effects of the supporting structure which can also be realized by fabrication where the radial extent of the optical mode is much smaller than the inner diameter of the torus.

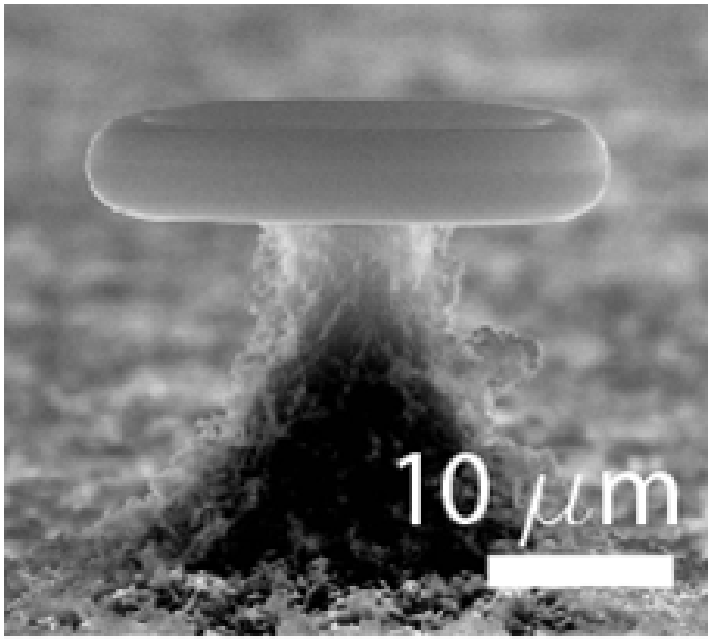

Figure 1.3: Scanning electron microscope image of a microtoroid.

Then the solutions for 1.5 for microtorid geometry is of similarity to that of the microsphere geometry with further spatial confinement. The derivations for microsphere optical modes have been obtained in several attempts. These derivations and the closed form expressions of optical modes in a microsphere are explained in detail in Appendix A. A microsphere or a microtoroid can be used as a transducer for sensing biological target probe molecules or particles via their optical resonances. Through functionalization of the microcavity surface target probes can be immobilized, then the evanescent fields of optical modes (λ) in the cavity interact with the target probes which in fact perturbs ($\delta\lambda$) the authentic optical modes. There are two possible mechanisms for detecting molecules/particles with optical cavities. One is the **reactive shift** via which the detection is with a shift in the resonance wavelength. With the adsorption/binding on the surface of the microcavity, optical modes experience longer paths which results in a shift of the resonance wavelength ($\lambda+\delta\lambda$) to longer wavelengths. Target probe interacting with the functionalized cavity surface are recognized by their excess polarizability (α_{ex}) which is dependent on the size, shape and the refractive index. The reactive shift is expressed as

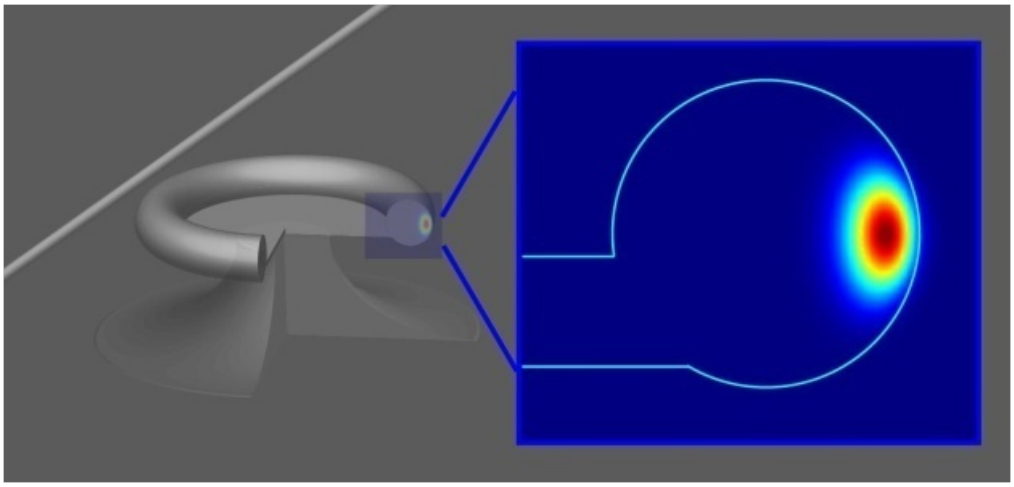

Figure 1.4: Simulated cross section of the microtoroid showing the location of the optical mode and the microtoroid geometry: Torus and the supporting structure.

$$\frac{\delta\lambda}{\lambda} \approx \frac{\alpha_{ex}\sigma_s}{\epsilon_0(n_1^2 - n_2^2)R} \tag{1.6}$$

where ϵ_0 is the vacuum permittivity, R is the orbital radius of the resonance, n_1 and n_2 are the refractive indices of the resonator and the surrounding, and σ_s is the surface density of the target probe molecule [27]. Resonance shifts provide extreme sensitivity to the amount of target probe on the resonator surface however they are also be sensitive to changes in the surrounding properties such as temperature, refractive index or particles/molecules in the resonance mode volume without adsorption.

The other mechanism for detecting particles/molecules with optical resonators is **mode splitting**. A particle adsorbed on the surface of the cavity with a certain polarizability scatters light into the degenerate mode propagating in the opposite direction in the cavity. In this case the particle on the resonator surface lifts the degeneracy of clockwise and counter-clockwise propagating modes. The result is two standing wave modes with slightly different resonance frequencies. Splitting between the two standing wave modes provides information about the size, shape and the refractive index of the particle. Analytically such a splitting in frequency is described as

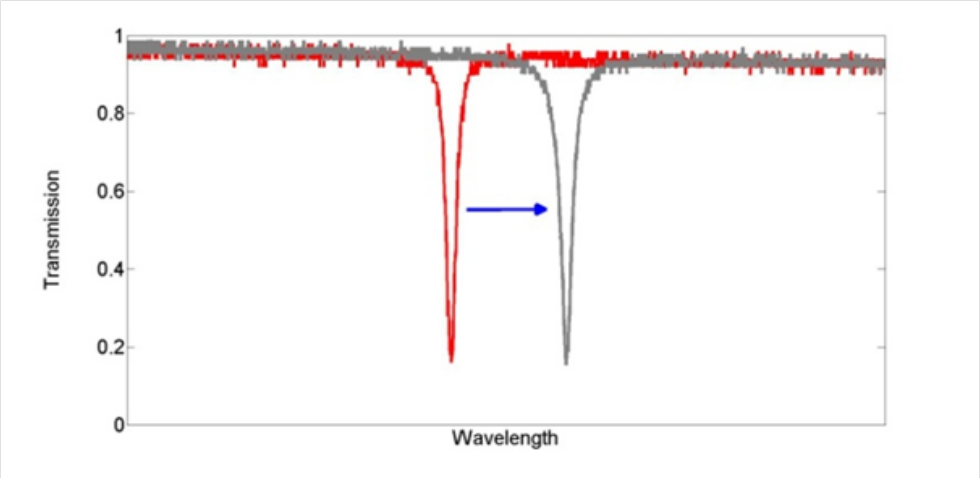

Figure 1.5: Biosensing with reactive shift in the optical modes of a microcavity.

$$g = -\frac{\alpha(f(r))^2\omega_c}{2V_c} \tag{1.7}$$

where ω_c is the angular resonance frequency, $f(r)$ is the normalized mode distribution, V_c is the mode volume and α is the particle polarizability which can be calculated practically from a measurement (or estimated from the known particle refractive index, size and shape) and can provide size information about the particle. Mode splitting can only be caused by particles on the resonator surface therefore cannot be observed by surrounding changes however practically requires a certain size or polarizability for the particle to be observed [35]

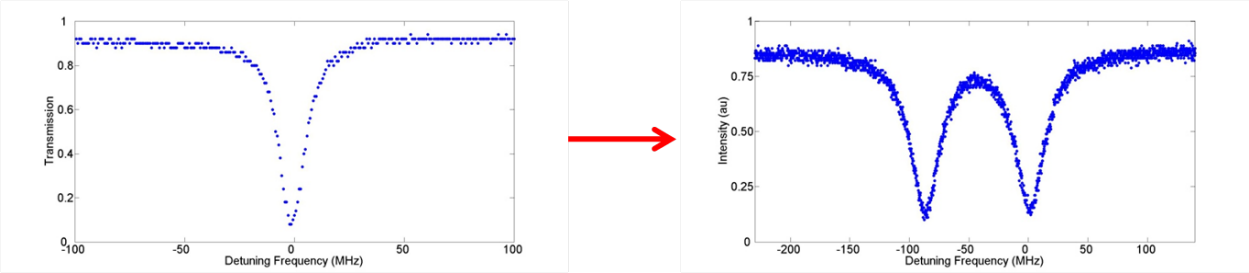

Figure 1.6: Biosensing with mode splitting.

Resonance shifts in aqueous environments are extremely sensitive to changes in the surroundings of the resonator however the total amount of measured shift may not only be

caused by particles on the resonator surface but can be due to temperature fluctuations and other noise mechanisms. On the other hand mode splitting scheme can detect single target probes and provide self-referenced information about the detected target probes but lacks the ability to detect and characterize below polarizability threshold target probes in ensemble amounts. In the following sections, biosensing is realized making use of both resonance shifts and mode splitting phenomena where surrounding refractive index changes and low polarizability target probe molecules are detected with resonance shifts and observation of splitting in the optical modes are attributed to additive behavior of target probe molecules. It is believed that such an analysis takes one more step towards single molecule detection with optical microcavities [13].

1.3 Experimental Setup

Throughout the experiments performed for this thesis excitation of the optical modes in the microtoroids is via tapered optical fiber (Fiber taper). Fiber taper is the most efficient method for exciting optical modes in a microcavity. In order to monitor the optical mode in real time a tunable semiconductor diode laser is used. Output signal is collected with a photodetector and monitored in real time on the oscilloscope. The use of microtoroids as biosensors requires them to be placed in aqueous environments. Along with its advantages in sensitivity and real time monitoring, biosensing with a micron-size transducer has drawbacks. When single molecule sensitivity is set as the goal, extremely low concentrations is required for resolution of single binding events within the instrument limited data acquisition in real time measurements. In low concentration environments diffusion is also slow which leads unpractical measurement times. On the other hand, a certain number of events are also desired for the validity of single molecule/particle measurements. Together with long-time measurements acquiring desired amount of single binding events then become an impossible task. Such difficulties can be overcame with the use of a microfluidic system, appropriate tubing and syringe pumps. Therefore the experimental setu and sample preparation consists of fabrication of microtoroids and fiber taper, microtoroid functionalization, microfluidic system and data acquisition.

1.3.1 Microtoroid Fabrication

Microtoroids are fabricated from silica. Optical properties such as low loss in near infrared, visible and telecommunications wavelengths along with well established fabrication processes make silica a good choice of material as an optical microcavity. Fabrication of silica microtoroids are through basic lithography using commercially available $2\mu m$ thick thermal oxide on $1mm$ thick circular silicon wafers of 3" diameter.

As shown in Figure 1.7, silica pads are created by photolithography. First, silica surface of the wafer is dried on a hot plate for 5 minutes for dehydration of the surface. Then the surface is spin coated at 2000 *rpm* for 10 *seconds* with a reagent (Hexamethyldisilazane, 98+% Alfa Aeser) to promote the adhesion of the photoresist. Making use of the reagent,

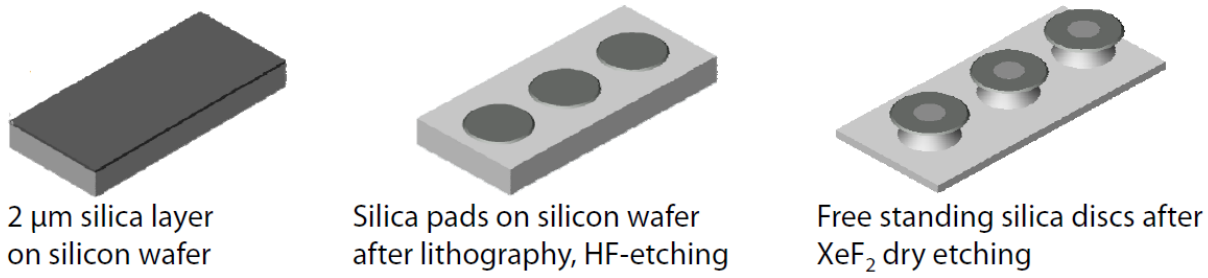

Figure 1.7: Fabrication of silica microdisks from 2 μm thick thermal oxide silica layers on silicon wafers.

the surface is then coated at 3000 rpm with photoresist (S 1813, Shipley Microposit) and baked for 1 min at 115 C° before exposure to UV. Using a mask with several sizes of circular patterns, wafer is exposed to UV while in contact with the mask. Later the photoresist is developed (MF 319, MicroChem Corp.) and the photoresist coated circular patterns are baked for 3 $mins$ at 115 C°. When wet etched with buffered hydrofluoric acid excess silica is etched away and the resulting pattern consists of circular pads (Figure 1.7, middle).

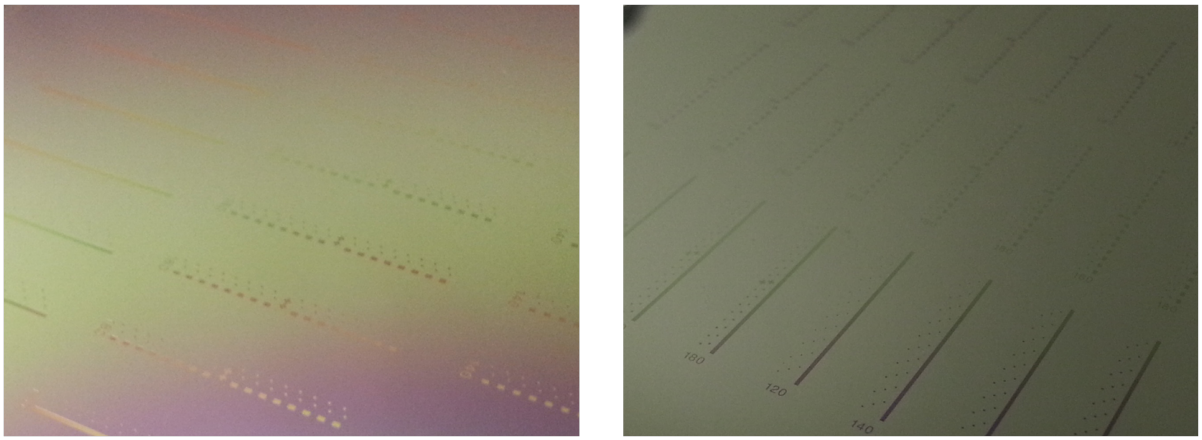

Figure 1.8: Before (left) and after (right) wet etching of the lithographed silica wafer. Size of the circular pads range from 100 to 180 μm

Once the circular pads of the needed size are obtained, the photoresist is washed away with acetone and the wafer is cleaned with isopropanol and water. Then, wafer is cut into smaller pieces for dry etching with $XeFl_2$. After dry etching silica microdisks are obtained.
Microtoroids are formed by reflow of the microdisks with a CO_2 laser operating at 10 μm

wavelength where silica has strong absorption. Reflow is then by heating of the silica microdisk with the CO_2 laser. By adjusting the power, the major and minor diameters of the torus can be varied. Precise control of these parameters provide fabrication of ultra high quality factor (10^8) microtoroids with preservation of the quality factor in aqueous environments (10^7). In general, major diameter is selected as 80 to 100 μm where the minor diameter ranges from 2 to 4 μm. Such a choice provides the smallest mode volume for optical resonances while maintaining the required quality factor for single molecule sensitivity.

1.3.2 Fabrication of Fiber Tapers

In optical microcavities coupling is one of the major challenges. For this reason various coupling schemes have been proposed such as buried waveguide coupling, prism coupling, angle polished fiber prism coupling, optical fiber half coupling and tapered fiber coupling all of which have advantages and drawbacks in either efficiency or robustness.

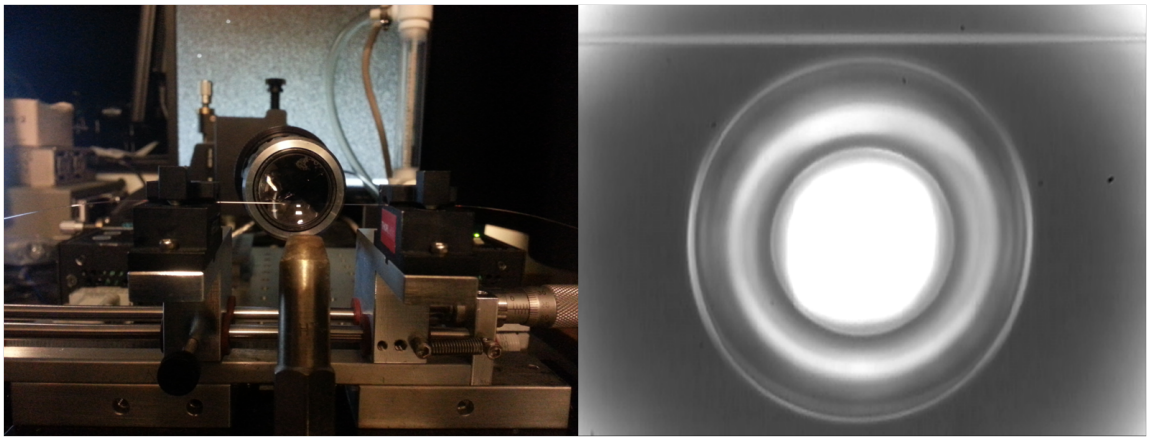

Figure 1.9: Fiber taper pulling stage showing the fiber held with clamps and the hydrogen flame source (left). Optical microscope image of the top view of the fiber taper next to a microtoroid (right).

In this work tapered fibers are used. Contrary to expectation, fiber tapers have proven to be robust enough throughout this work for use in aqueous environments with external flows provided by syringe pumps. Tapered fiber coupling provides $\sim 100\%$ efficiency and supports the control of the gap between the microtoroid control. The gap between the fiber taper and the microtoroid is controlled with a 100 nm resolution 3-dimensional piezo stage. Tapered

fibers are fabricated by heating and pulling of a single mode optical fiber using a hydrogen flame. The transmission through the fiber is monitored as the fiber waist gets thinner. Once a spatially single mode transmission is achieved pulling and heating of the fiber is stopped and the desired thickness is achieved in the tapered portion of the fiber.

1.3.3 Microfluidic Chamber and the Flow System

As explained in the earlier sections a microfluidic flow system is required for the transport of extremely low concentrations of target probe molecules onto the functionalized microcavity. A good choice of material to enclose the silica microtoroid chip and the fiber taper in the solution while minimizing the contamination and other effects. For this reason, polydimethylsiloxane (pdms) chambers have been fabricated.

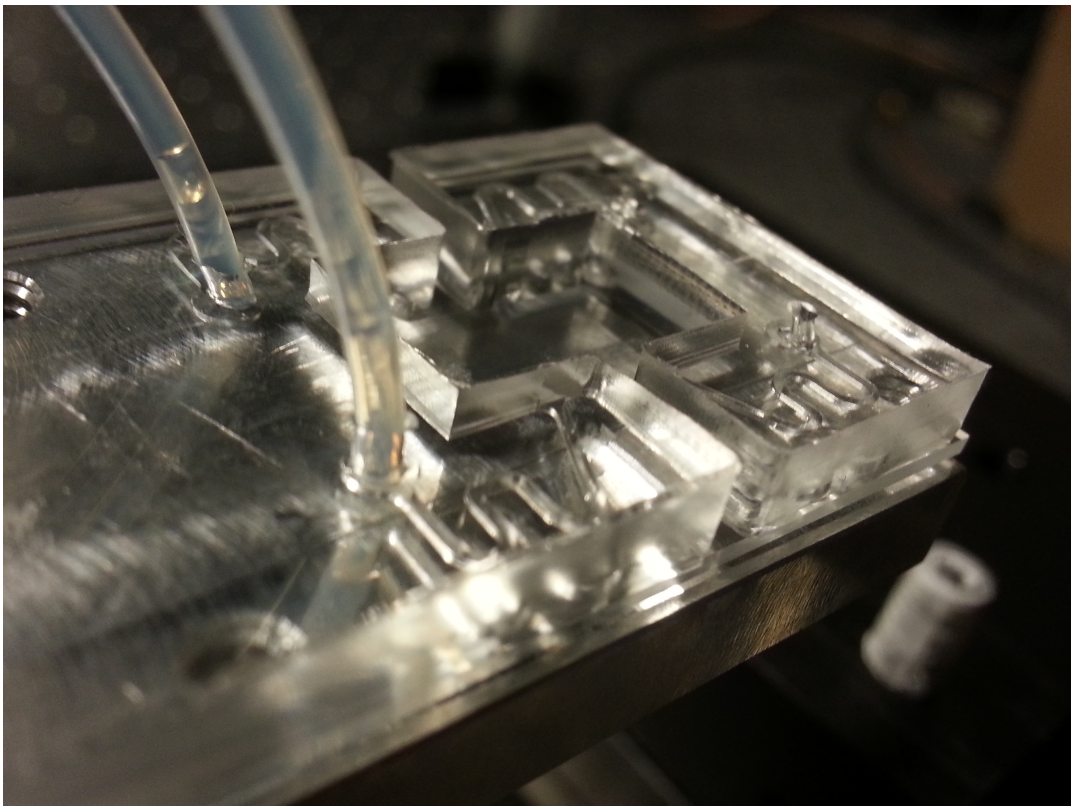

Figure 1.10: PDMS microfluidic chamber with two inlets and two outlets. The slits are for controlling the gap between the fiber taper and the microtoroid.

Bio-sensing experiments with microtoroids are performed in aqueous (buffer). Two of the syringe pumps are used for insertion and extraction while maintaining a constant flow of the aqueous (buffer) solution. The experiments are performed with different concentrations of target probes. In order eliminate non-specific binding/adsorption of the target probe flow of the buffer solution is kept constant. Microtoroid is placed in the chamber and then the chamber is filled with Phosphate Buffered Saline (PBS) solution of pH 7.5 and volume 0.8 ml and target probe molecule solutions (also in PBS) are added with a micropipette while monitoring the transmission. Thermal effects are reduced by keeping constant flow at 0.3 ml/min of PBS buffer which also provides cleaning of the microtoroid and therefore avoids nonspecific binding and adsorption since the aim of this experiment is to demonstrate specific binding with a functionalized microtoroid surface.

1.4 Functionalization with Genetically Engineered Peptides and Measurement of Peptide Streptavidin Interaction

This section presents the experiments performed with microtoroid optical cavities with an efficient and easy functionalization method using genetically engineered peptides (GEPIs). GEPIs provide inorganic-binding and assembly properties for a variety of applications such as materialization, molecular medicine, and energy systems [22]. GEPIs can bind specifically to solid materials and the existence of a well established characterization for binding kinetics and specificity makes them reliable molecular tools for molecular targeting and sensing [23]. For a proof of principle experiment, a most conventional and strong non covalent binding pair of molecules (biotin-streptavidin) was chosen. Biotinylated silica binding peptides are used to functionalize the ultrahigh quality factor microtoroid cavities to specifically detect streptavidin. Functionalization was performed under continuous monitoring of the device performance in aqueous environment. In order to verify the performance of GEPI with the silica microtoroid resonator, dye conjugated streptavidin molecules are used in fluorescence microscopy.

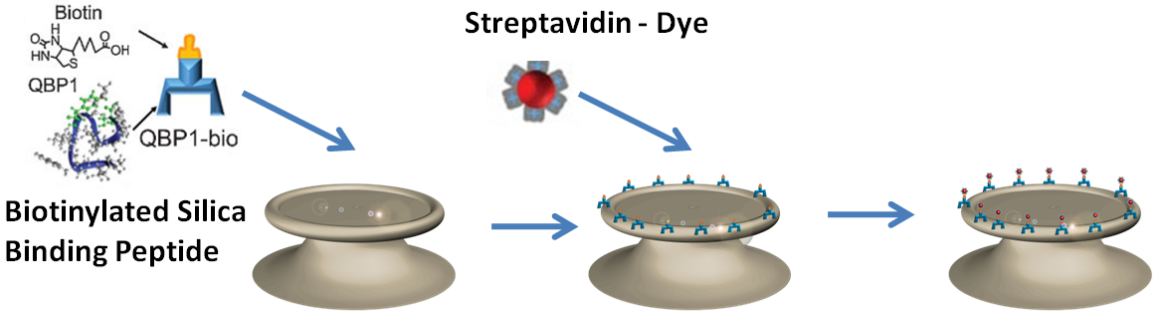

Figure 1.11: Illustration of the functionalization of microtoroid cavities with biotynilated silica binding peptides and the detection of streptavidin.

Functional surface chemistry was easily achieved with GEPIs without any costly rigorous treatments and the microtoroid resonator was as efficient as before functionalization. For the device performance, quality factors are measured during functionalization with GEPIs. Later, streptavidin was sensed with not just conventional resonance shifts [27] but also via

mode splitting which has become a powerful platform for single molecule sensing. The results of the experiments shown here are encouraging towards specific single protein detection.

1.4.1 Functionalization with GEPIs

The first step of the experiment is monitoring the functionalization of the microtoroid with biotinylated silica binding peptides. GEPI functionalization was monitored by continuously measuring the changes in resonance wavelength as peptides are introduced into the chamber where conventional functionalization methods require preparation of functionalized optical cavity surfaces through chemical processes without the real time monitoring of the effects. As the peptides bind to the toroid, resonance frequency shifts finally reaching saturation. The chamber was continously purged with the buffer solution to eliminate the effects of weakly bound or non-specifically adsorbed peptides. The net resonance shift is due to strongly bound peptides.

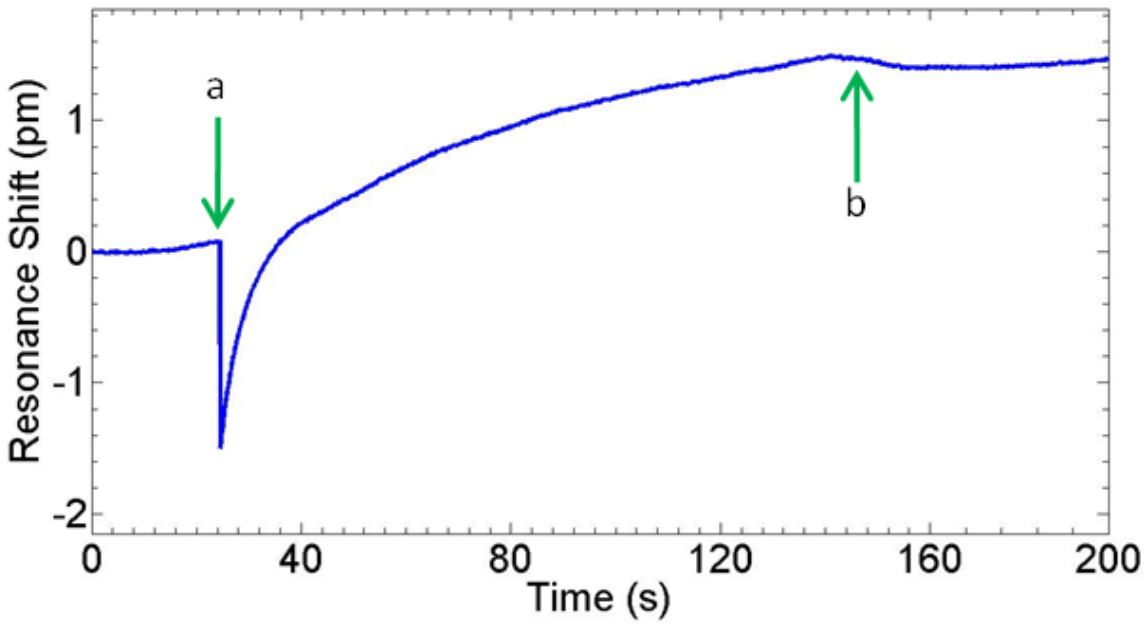

Figure 1.12: Spectral position of the resonance while GEPIs are added to the solution. Addition of the GEPIs causes a sudden thermal shift (indicated as **a**). Saturation of the shift due to binding of GEPIs is indicated as **b**.

In order to minimize thermal effects during resonance shifts due to GEPIs are added with small volumes (2 μl) using a micropipette. In figure 1.12, final concentration of the GEPIs are $10nM$. Since GEPIs are used for functionalization, small concentrations are not necessary, rather for an achieving an efficient biosensing element maximum available surface coverage of GEPIs is aimed. For this reason, microdroplets of high concentrations are added to the chamber until the resonance shifts saturated.

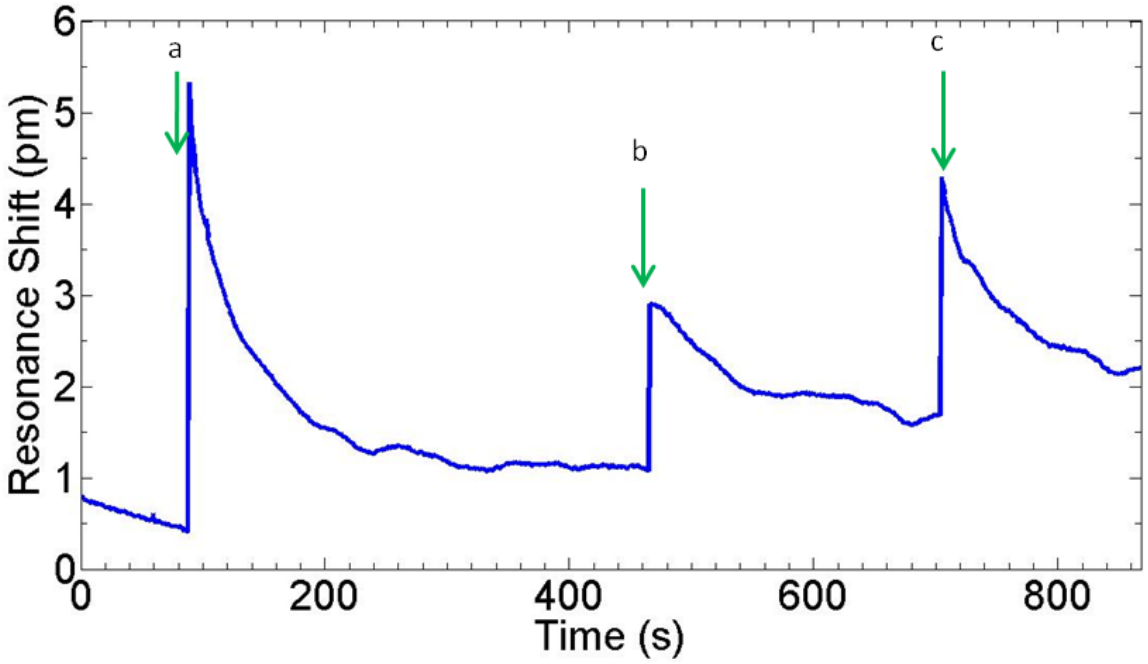

Figure 1.13: Spectral position of the resonance with the addition of different concentrations of GEPIs. **a**, **b** and **c** indicate the addition of the microdroplets into the chamber.

It is important to note that sudden thermal shift with the addition of the GEPIs in buffer can cause a temperature increase as well as a decrease. Increase of the temperature in the chamber results in a shift to longer wavelengths where the decrease causes shift of resonance to shorter wavelengths. Figure 1.13 shows the addition of increasing concentrations of GEPIs. A resonance shift of 0.7 pm is observed with addition of $3.33nM$ GEPIs solution at point **a**. Then the concentrations is increased in steps to 10 nM and 20 nM where the observed shifts are 0.6 pm and 0.5 pm. Higher concentrations yielding to smaller resonance shifts is indicative of saturation of the surface of the microtoroid with GEPIs. The density of the GEPIs on the surface of the silica microtoroid are limited by the affinity of the GEPIs. In order to estimate the saturation concentration of GEPIs, surface densities obtained in

previous studies involving similar protein structures are used which yields to concentrations of about 20 nM. Measurements with higher concentrations (100 nM to 1 μM) only caused resonance shifts of about 1 pm which correlates with the estimated saturation concentrations.

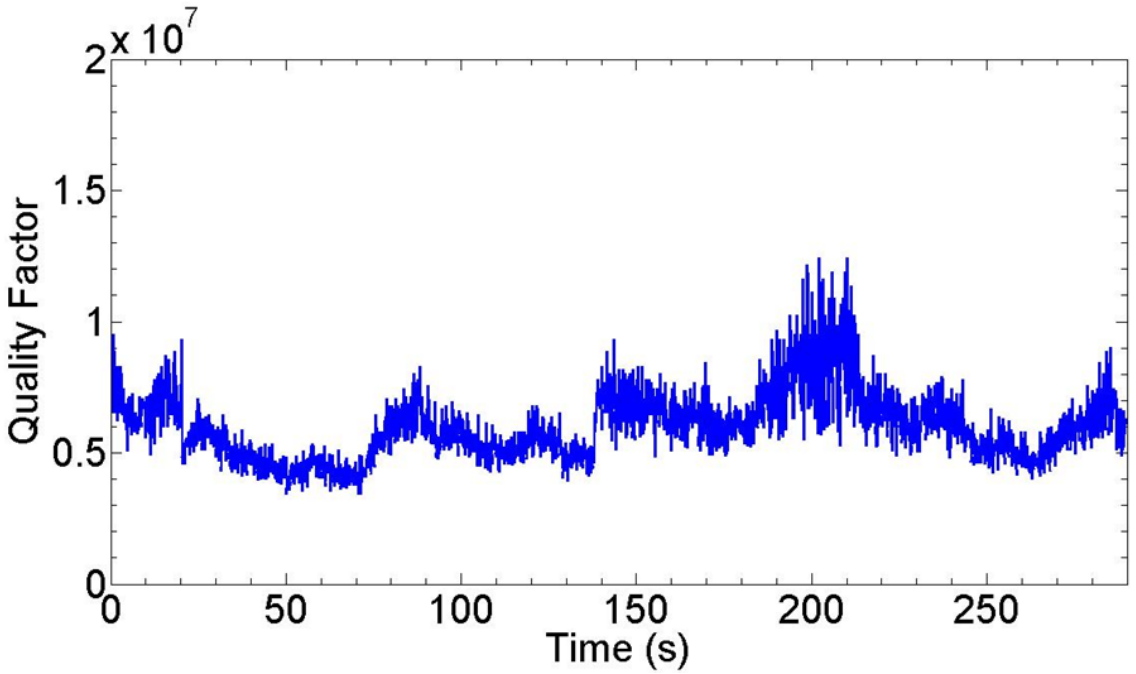

Figure 1.14: Quality factor of the resonance throughout the functionalization process as a function of time.

As proposed in the beginning of this section, the aim of functionalization with GEPIs is to obtain an efficient biological sensing element while maintaining the sensitivity of the transducer. Therefore throughout the functionalization process quality factor of the microtoroid cavity is measured. Figure 1.14 shows that the initial quality factor ($\sim 10^7$) is maintained. Fluctuations in the quality factor is due to fiber taper - microtoroid coupling fluctuations which is fixed occasionally using the piezo control. Note that the quality factor measured here is $1/Q_{intrinsic} + 1/Q_{coupling}$.

1.4.2 Streptavidin Measurements

Once the binding of peptides is confirmed, the next step is to detect streptavidin molecules and hence biotin-streptavidin binding. A very important feature of this experiment is the

real time monitoring of the functionalization of the silica microtoroid which has not been attained with previous functionalization methods [10]. Furthermore the quality factor of the resonator has not deteriorated. In the second part of the experiment, different concentrations (1 nM and 2 nM) of streptavidin is added in the same way with a micropipette using the same volume, 2 l. Note that streptavidin concentrations are 10 times smaller with respect to the GEPIs concentrations. This is due to the binding rate of biotin:streptavidin (1 : 4 to 1 : 10).

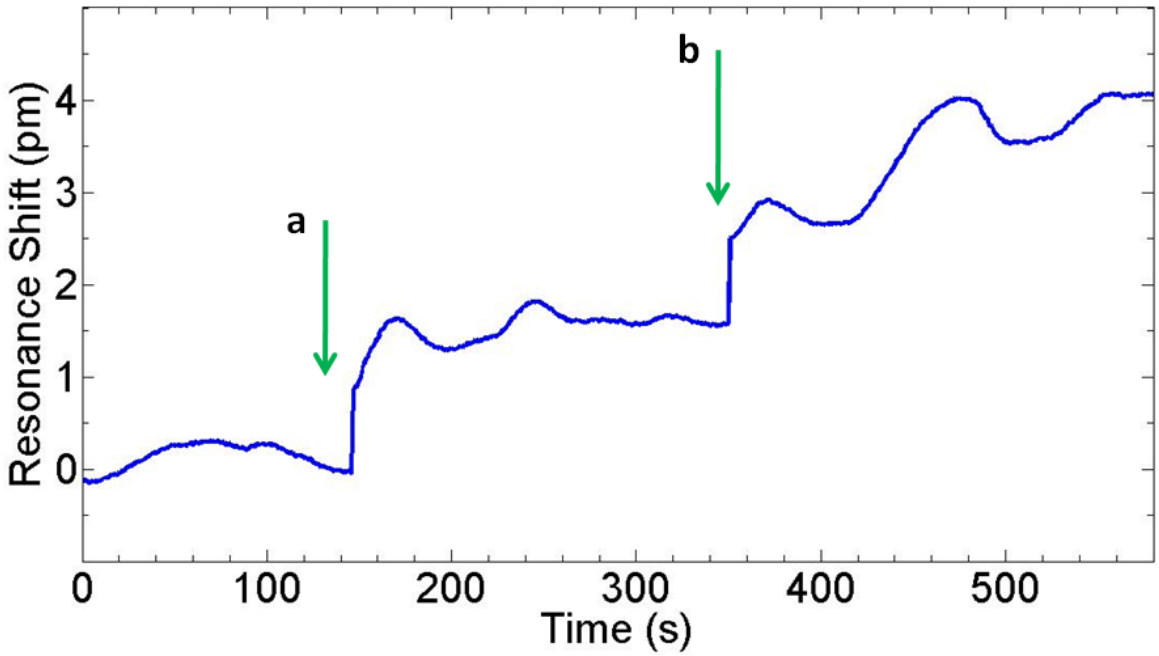

Figure 1.15: Spectral position of the resonance as different (indicated as **a** and **b**) concentrations of streptavidin solutions are added to the solution.

As streptavidin is added into the solution resonance shifts of 1.6 pm and 2.5 pm are measured. Since the polarizability of streptavidin is bigger than the polarizability of GEPIs, the resonance shifts induced by streptavidin are larger.

Detection of biotyn-streptavidin binding, BSA protein and similar biological interactions have been studied using optical microcavities recently. However, single molecule detection or single events of such biological structures has not been reported as of yet. Since the GEPIs functionalization allows detection of bio-molecules with single events, a new set of experiments are performed with the same method of functionalization but with the search of mode splitting instead of resonance shifts. The excess polarizability of streptavidin is $4\pi\epsilon_0$

(3.3×10^{-21}) [34], which theoretically corresponds to a mode splitting (via equation 1.7) of 0.04 MHz with the assumption that streptavidin resides at the field maxima, $f(r) = 0.36$. However such a splitting is beyond the limit of detection with even ultrahigh quality factor resonators. Nevertheless, multiple streptavidin molecules residing on a scattering site could result in a gradually increasing mode splitting over time course without single binding events. Therefore, a resonance with an authentic linewidth of 10 MHz (easily attainable with microtoroid cavities) could refer to detection of a minimum number of 250 streptavidin molecules with an ideal condition that all of the streptavidin molecules reside at the same field maxima.

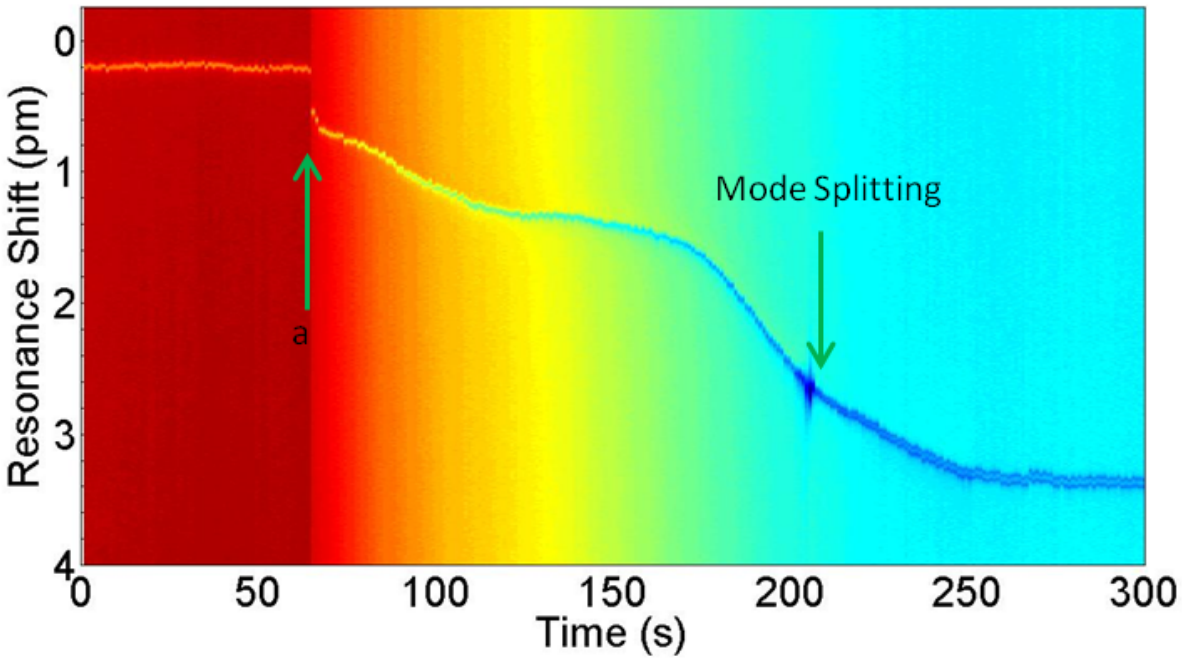

Figure 1.16: Spectral position of the resonance with addition of streptavidin solution indicated as **a**. Start of the splitting in the resonance mode is indicated. Color code indicates the intensity of the transmisison.

For the second set of streptavidin detection experiments the changes in the resonance is monitored and the moment of splitting is recorded (Figure 1.16) as Streptavidin solution is added into the chamber to achieve a concentration of 300 fM. At the first measurable instant the mode splitting is 15 MHz. The gradual increase in the mode splitting indicates that single streptavidin molecules can not be detected however the time evolution of the

mode splitting provides information about the minimum number of streptavidin molecules detected.

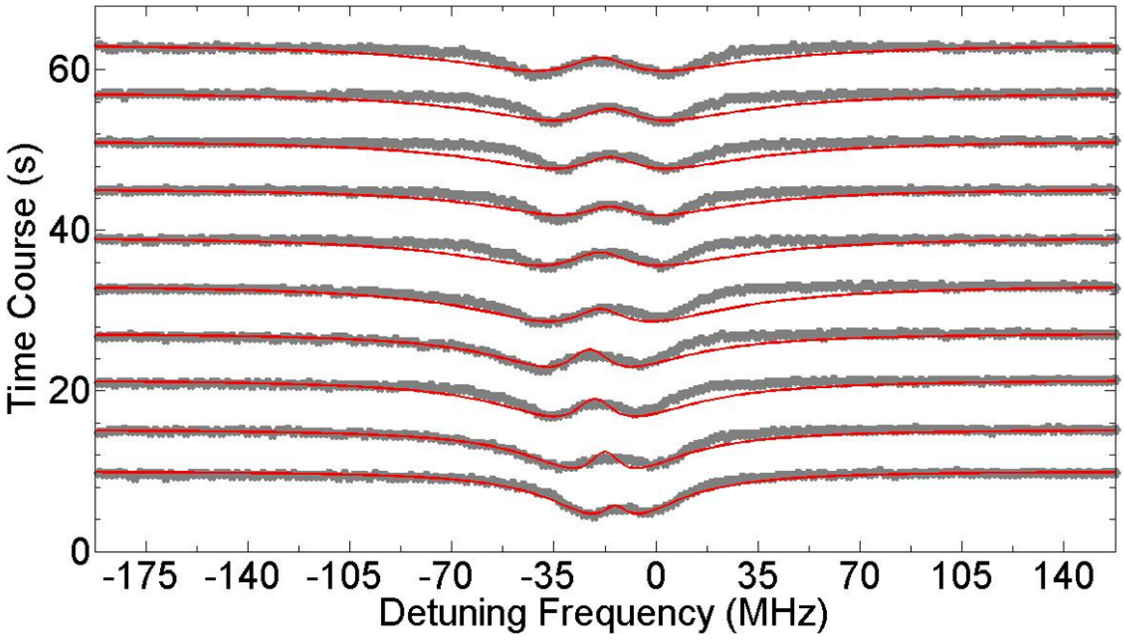

Figure 1.17: Evolution of mode splitting as it increases as more streptavidin molecules bind to the scattering point.

In Figure 1.17, the evolution of the mode splitting in time is presented. Mode splitting increases from 15 MHz to 44 MHz. We estimate that this amount of change in splitting is due to the several hundred of Streptavidin Biotin binding events. It is important to note that the increase in the mode splitting is faster in time (¿1 min) than the observed resonance shifts (5-10 mins) as expected since the number molecules detected via mode splitting phenomena is much less than the number of molecules detected with a saturated resonance shift. In fact each of the ten transmission curves plotted in Figure 1.17 show different amounts of splitting in frequency. The minimum number of streptavidin molecules detected in between each transmission curve acquisition is around 100. Biosensing demonstrated in this work with ultrahigh quality factor optical resonators outperforms the previous studies [27, 10], for two reasons. First is the hybrid sensing technique used: Combining the advantages of reactive shift and mode splitting phenomena extreme sensitivity is obtained while eliminating the noise sources such as temperature which is substantial as the detected number of molecules gets smaller. Second is that, GEPIs functionalizatoin provides to our knowledge highest sensitivity with a functionalized optical microtoroid cavity.

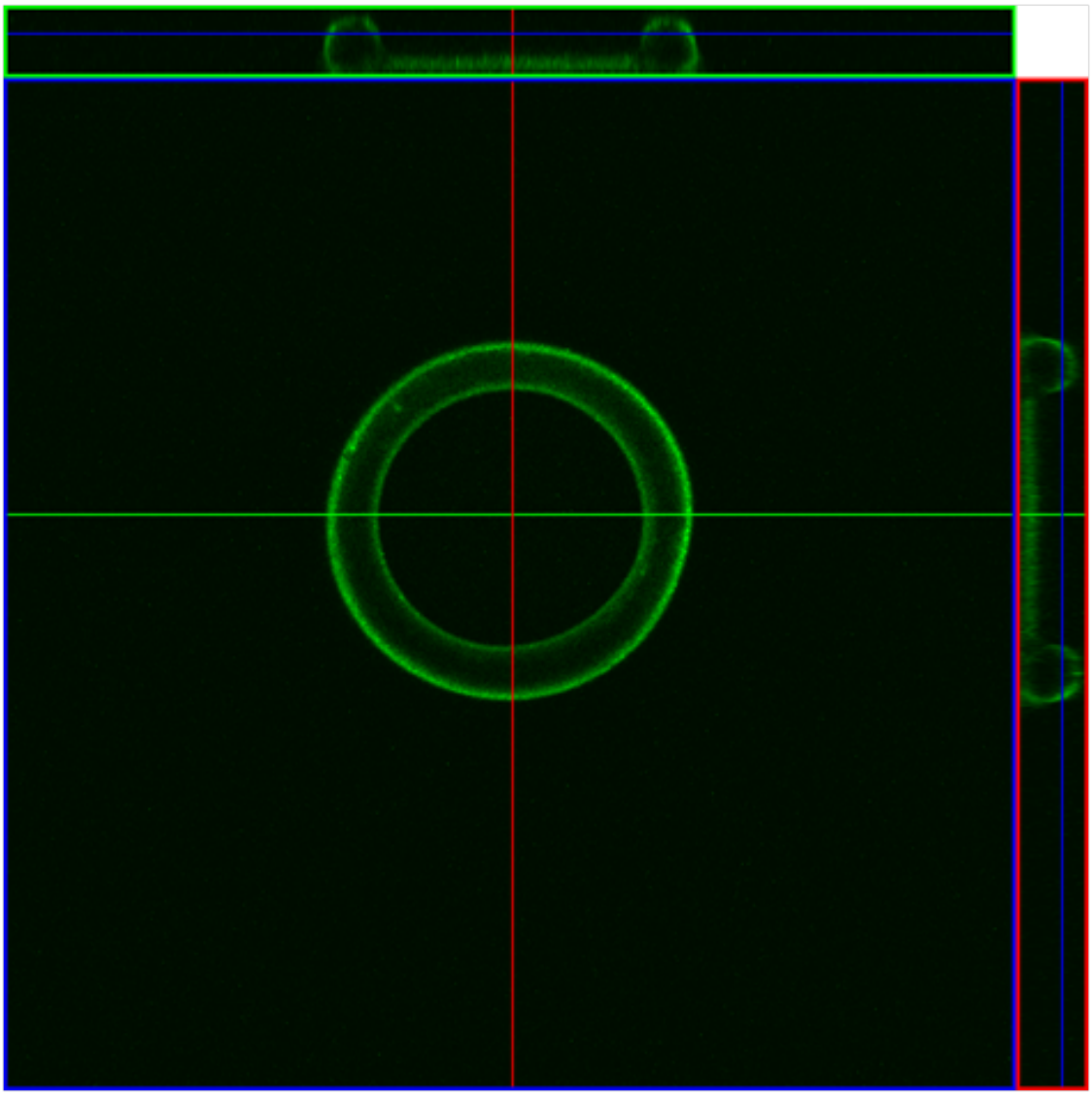

Figure 1.18: Fluorescence microscopy image of the microtoroid and projected cross sections (on top and the right of the image) treated with GEPIs and dye conjugated streptavidin.

In order to test the binding kinetics of biotinylated silica binding GEPI and the silica microtoroid and to confirm the efficiency of functionalization dye conjugated streptavidin molecules are monitored with confocal fluorescence microscopy. First, microtoroids are placed in the buffer solution of GEPIs. Then the microtoroids are washed with buffer solution. Later, microtoroids were placed in dye conjugated streptavidin solution and after a few seconds again washed with the buffer solution in order to prevent nonspecific binding. As a control experiment, microtoroids with no functionalization (no GEPIs) were also treated with dye

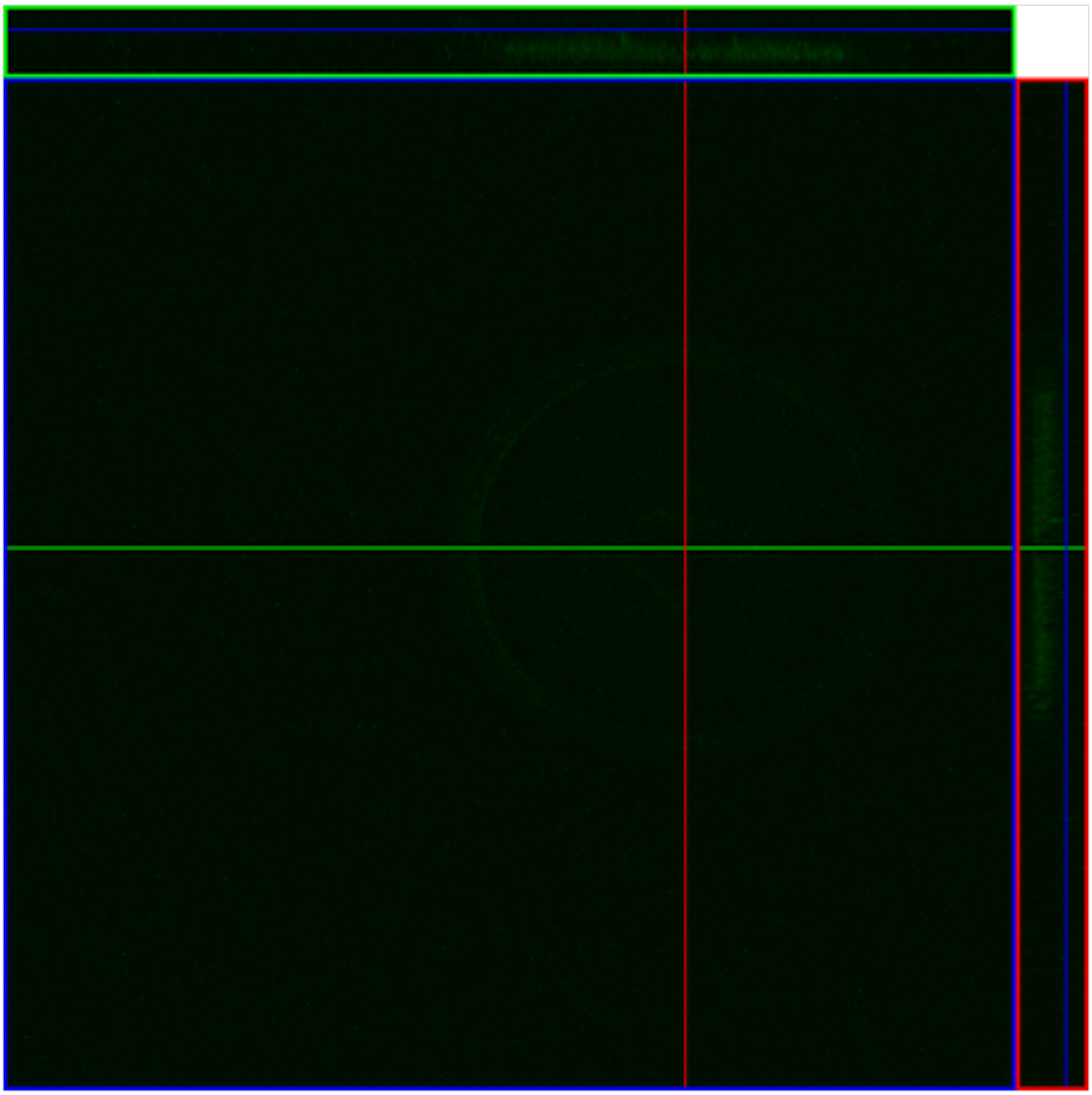

Figure 1.19: Fluorescence microscopy image of the microtoroid and projected cross sections (on top and the right of the image) treated with only dye conjugated streptavidin.

conjugated streptavidin with the same procedure. Figure 1.18 shows the projected cross section images that provide information about the exact location of the source of the biotin-streptavidin binding sites since the streptavidin is the fluorescence source. Since the support structure of microtoroids (pillar) is also made of silica, they also serve as binding sites for GEPIs. Nonetheless, the brightness of the torus part of the microtoroid indicate that the dye conjugated streptavidin is present on the resonator surface.

Figure 1.19 shows the image collected from one of the control microtoroids. The lack of

fluorescence from the torus part of the microtoroid is a clear indicative of absence of streptavidin on the resonator surface. Hence the fluorescence obtained in figure 1.18 is not due to the nonspecific binding of streptavidin to silica but due to the biotin-streptavidin interaction. Furthermore the latter is also evidence for the successful surface modification of silica microtoroids with GEPIs.

Chapter 2

Nanoparticle Detection using Fiber Tapers in Aqueous Solutions

2.1 Fiber Tapers as Transducers

Along with the advances in industry and technology the amount of nanoparticles synthesized or produced secondarily have increased greatly along with the demand for their detection and characterization. Nanoparticles -ultrafine particles- are 1 to 100 nm in size and range from virions to semiconductor and metal secondary products. Therefore nanoparticle detection is not only essential in biodefense but also in their wide range of applications ranging from medicine to energy, electronics and optics. Common techniques for nanoparticle characterization include electron microscopy (TEM, SEM), atomic force microscopy (AFM), dynamic light scattering (DLS), X-ray photoelectron spectroscopy (XPS), powder X-ray diffraction (XRD), Fourier transform infrared spectroscopy (FTIR), ultraviolet-visible spectroscopy and nuclear magnetic resonance (NMR). Even though such conventional methods provide information about the nanoparticle properties and synthesis all of them lack the ability to detect and characterize single nanoparticles in real time measurements without labels.

Optical microcavities offer extremely high sensitivity in detection of biological targets and nanoparticles however they require use of highly stable and tunable laser sources, precise control of frequency with electrical components and light coupling mechanisms that require nanometer scale resolved control of position. Therefore optical microcavities are still far away from real life practical applications. On the other hand, interest in nano/micro-scale

sensors for nanoparticle/biomolecule detection is expanding due to their remarkable sensitivities. This chapter is dedicated to present nanoparticle detection using a very simple submicron-scale sensor that has the ability to work with only a single frequency light source while preserving the sensitivity of considerably more complicated sensor systems.
As explained in the previous chapter, fiber tapers have the ability to expose light to the surrounding environment which makes them excellent tools for light coupling. In addition to their use with optical microcavities, fiber tapers have also been explored for their potential use as evanescent field based sensors. Recent efforts have demonstrated that fiber tapers are highly sensitive offer a cheap and compact sensing platform. Here fiber tapers are used as transducers for detection of single nanoparticles in aqueous solutions [36].

2.2 Detection Mechanism

Detection of molecules/nanoparticles using fiber tapers is based in loss introduced by the target probe to the intensity of the light transmitted through the fiber. Such a loss is due to the light scattering from the target probe. In the case of a biomolecule or a nanoparticle, while operating wavelengths are within visible, near infrared or telecommunications bands, the size of the target probe is much less than the wavelength of the light. When the size of the scatterer (d) is much less than the wavelength (λ) of light, the principle is called Rayleigh scattering. According to Rayleigh scattering, the intensity of light scattered by a spherical particle in air is given by

$$I = I_0 \left(\frac{1 + \cos^2(\theta)}{2R^2} \right) \left(\frac{2\pi}{\lambda} \right)^4 \left(\frac{\varepsilon_{particle} - \varepsilon_{medium}}{\varepsilon_{particle} + 2\varepsilon_{medium}} \right) \left(\frac{d}{2} \right)^6 \tag{2.1}$$

where I_0 is the incident light intensity, θ is the scattering angle, R is the distance from the particle, λ is the wavelength of the light, ε is the permittivity and d is the diameter of the particle. When the intensity drop in the light throughput is measured sum of all the angles is considered. Most importantly, the scattered light intensity depends on d^6/λ^4. In fact, scattered light intensity is proportional to the second power of the polarizability (α) of the target probe where for a spherical particle

$$\alpha = 4\pi R^3 \frac{(\varepsilon_{particle} - \varepsilon_{medium})}{(\varepsilon_{particle} + 2\varepsilon_{medium})} \tag{2.2}$$

where in equation 2.2 R is the radius of the spherical particle.

2.3 Polystyrene Nanoparticle Detection

The experimental setup used in nanoparticle detection using fiber tapers is similar to the setup used in biosensing experiments in the previous chapter. The same microfluidic chamber is used without any flow of solutions of diluted PBS. Microfluidic chambers are fabricated from PDMS for each nanoparticle detection experiment to avoid contamination from previous experiments. Input light wavelength and intensity is kept constant throughout the experiment and the intensity of the throughput light is collected with a photodiode.

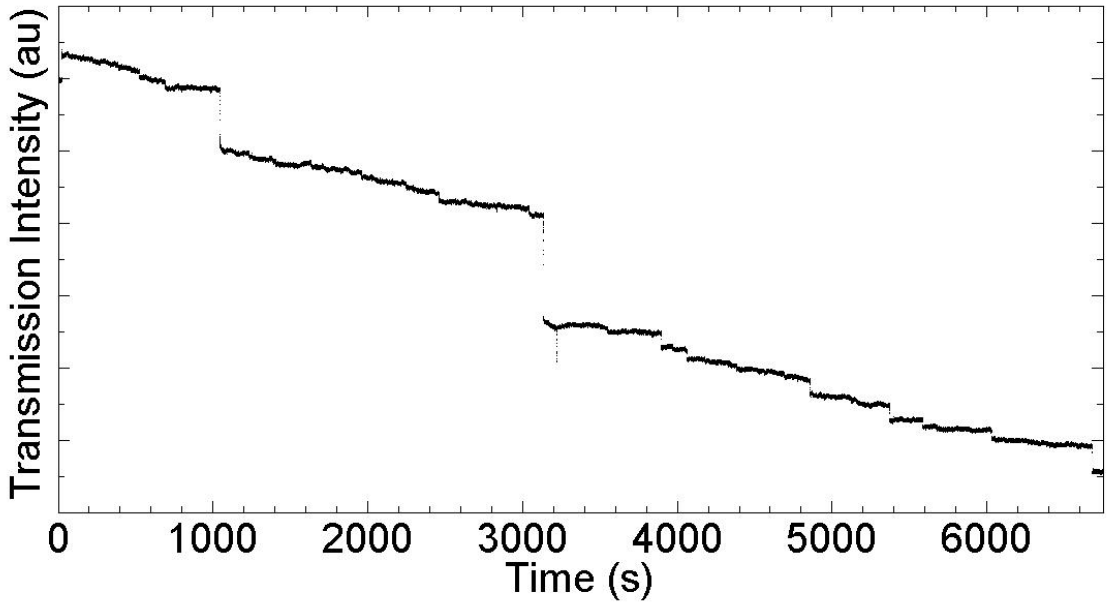

Figure 2.1: Transmission of the light through the fiber taper as PS nanoparticles bind to the fiber taper. Discrete drops in the intensity indicate single nanoparticles binding events.

Changes in the intensity are recorded using National Instruments data acquisition with a multichannel oscilloscope. In order to distinguish any intensity fluctuations from the light

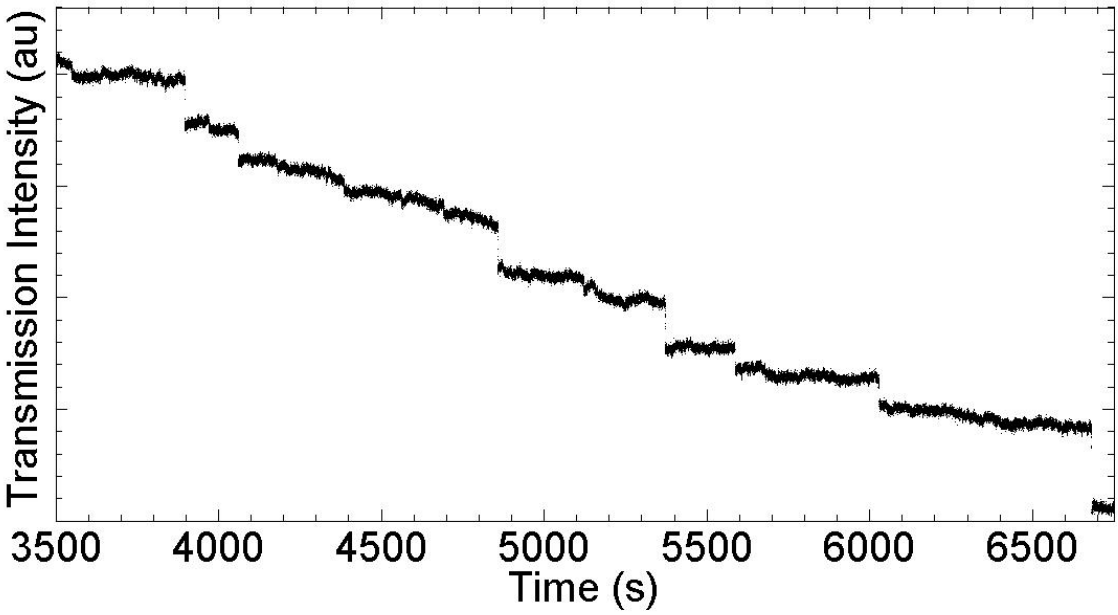

Figure 2.2: Closer look of the transmission showing several intensity drops through time.

source, intensity is measured and saved using a wavelength division multiplexer separate from the fiber taper.

Figure 2.1 shows the transmission of the light through the fiber taper over time as polystyrene nanoparticles (PS) of 60 nm diameter are added to the chamber. One of the advantages of detection with fiber tapers is the elimination of the thermal noise since the intensity of the transmitted light is immune to the changes in the temperature of the surrounding. Each intensity drop in figure 2.1 indicates a single PS nanoparticle binding to the fiber taper. Counting the number of intensity drops in the transmission provides the number of nanoparticles on the fiber taper. Height of the intensity drops is due to the intensity of the scattered light from the nanoparticles. According to Rayleigh scattering phenomena the intensity of the scattered light depends on the intensity of the incident light therefore the position of the nanoparticles on the fiber taper affects the height of the intensity drops since the waist of the fiber taper allows stronger evanescent fields where thicker parts allow weaker evanescent fields. Also, as more nanoparticles bind to the fiber taper the mode distribution is altered. Therefore the height of the intensity jumps depend on the distance between the nanoparticles as well as their location on the fiber taper waist. The change in the intensity due to a Rayleigh scatterer is proportional to α^2 and $(d/2)^6$. Therefore the changes in the

intensity are scaled to $1/6^{th}$ power and the number of at each intensity drop amount is shown in the histogram in Figure 2.3. To our knowledge, detection of nanoparticles as small as 30 nm in radius in aqueous solutions is shown here for the first time. In discovering the limits of the fiber taper nanoparticle detection system, 15 nm PS nanoparticles are also tested however the decrease in the intensity drop is expected to drop $6 - folds$ and such a small size proved to be beyond the detection limit of fiber tapers.

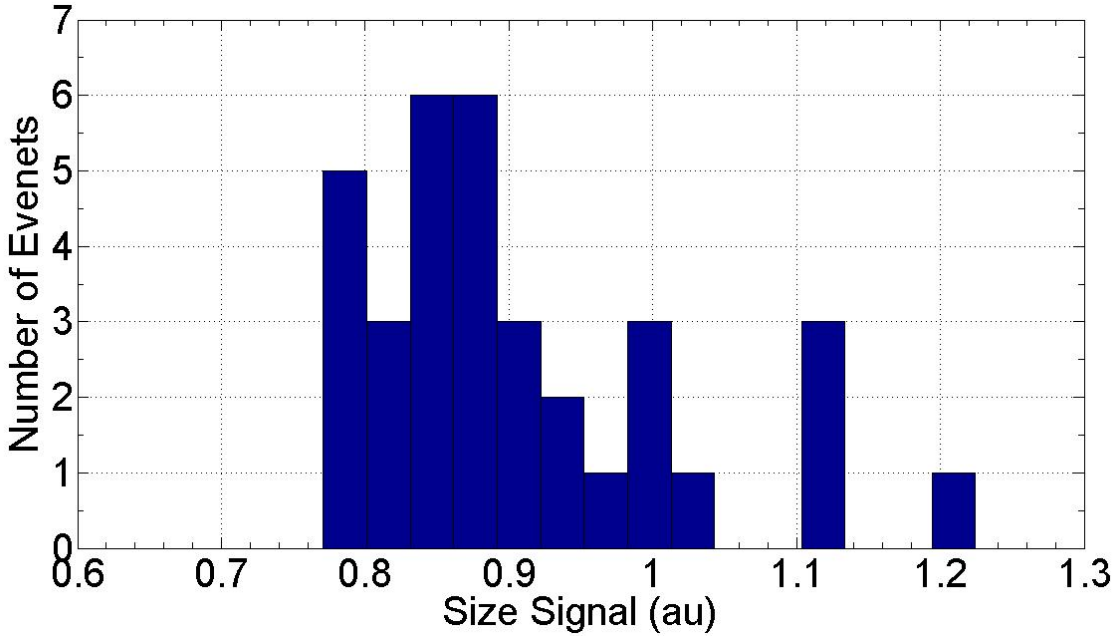

Figure 2.3: Size signal of the detected PS nanoparticles. The number of nanoparticles detected here is 34.

2.4 Gold Nanorod Detection and Plasmonic Enhancement

Gold nanoparticles have applications in cancer therapy and optoelectronic technology making use of their localized surface plasmon resonances (LSPR) with nanorod structures [1]. Gold nanorods provide easy tunability of LSPR allowing use of wide range of excitation wavelengths [21]. On the other hand localized hot spots due to surface plasmon resonance of metallic nanoparticles have shown to increase the sensitivity of optical microcavities. This

section aims to provide proof of principle experiments to demonstrate plasmonic enhancement of nanoparticle detection with fiber tapers. First, gold nanorods of 20 nm width and 60 nm length were synthesized with surface plasmon resonances centered around 660 nm. Then the detection experiments were performed with and without plasmonic excitation wavelengths in DI water.

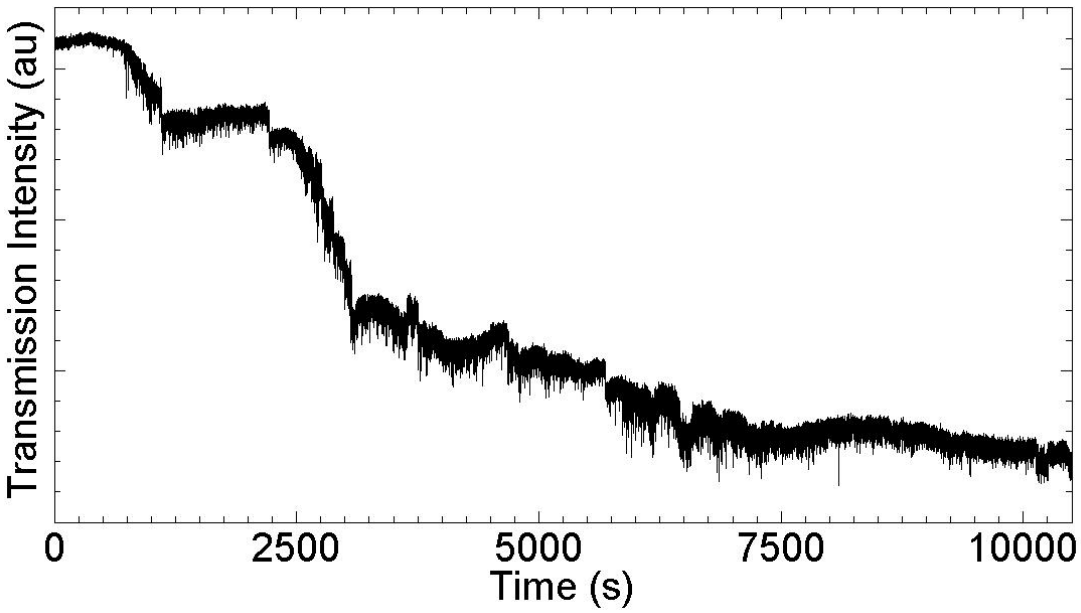

Figure 2.4: Transmission of the light through the fiber taper as Au nanorods enter the mode volume of the fiber taper. Aside from discrete drops in the intensity due to binding, sudden dips are observed with the help of plasmonic enhancement without binding.

Figure 2.4 shows the transmission of light through the fiber taper as gold nanorods are added to the chamber. Before the addition of the gold nanorods (500 *seconds*) the transmission does not exhibit dips. The infrequent and small number of intensity drops with gold nanorods (when compared to the PS nanoparticle events) is believed to be due to the lack of charges in the solution since instead of PBS buffer, de-ionized water is used to preserve the stability of the gold nanorods. However, gold nanorod detection showed a rather surprising result. Even without binding of the nanorods to the fiber taper, nanorods entering the mode volume generated changes in the transmission intensity. These changes were observed as dips in the transmission.

The nature of the dips in the transmission (only downward) distinguish themselves from electronic or optical noise since the nanorods are only expected to cause a drop in the transmission. The drops are however not permanent indicating that the binding is not efficient and in fact such behavior of the nanorods was observed from the optical microscope image of the fiber taper. A close look to one of the dips in the transmission reveals that a nanorod stays in the mode volume only for a few seconds. Confirmation of the plasmonic enhancement is via repeating the same experiment at non-plasmonic wavelengths. Therefore on a different experiment, same gold nanorods were detected using 1550 nm wavelength light.

Since the input light wavelength in this experiment is spectrally distant from the plasmonic resonance wavelength of the gold nanorods, no plasmonic enhancement is expected. This experiment reveals no temporary dips in the transmission. It is evident that evanescent field of 1550 nm light only allows detection of nanorods via binding where the infrequent behavior (small number of binding events over time) of the binding of nanorods repeats itself. Therefore the temporary dips observed at experiments operated at plasmonic resonance wavelengths is very likely due to plasmonic enhancement which is to say due to the absorption and the scattering of light from the nanoparticle.

In addition to the use non-plasmonic wavelengths as confirmation of plasmonicly enhanced sensing of gold nanorods, another experiment with different concentrations of gold nanorods using plasmonic wavelengths is performed. The purpose of this experiment is to observe a rather proportional increase in the number of temporary dips with increased concentration of gold nanorods in the chamber (Figure 1.7). Furthermore, post-processing of the transmission data (showing temporary dips with two different concentrations) reduced the noise level. By performing cross-correlation on the transmission intensity data and a step function in time domain Figure 2.8 is obtained. Figure 2.8 shows clear increase in the number of binding events as well as the amount of change in the intensity with increased gold nanorod concentration which is attributed to multiple nanorods binding between each data acquisition since the data acquisition is instrument limited and only allows a sampling rate of 50 ms.

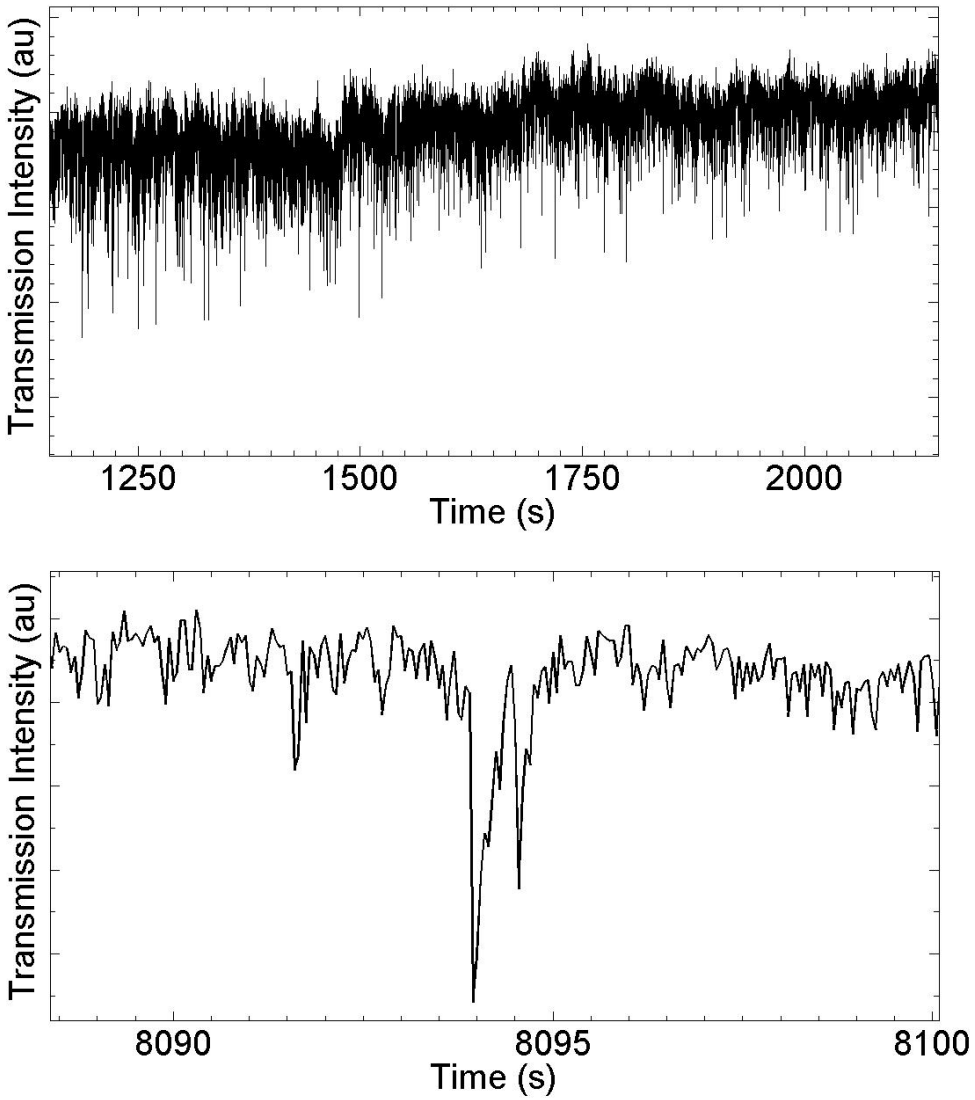

Figure 2.5: Dips in the transmission due to plasmonicly enhanced detection of gold nanorods (top). Time evolution of a single dip: Gold nanorod entering the mode volume is unable to bind and exits the mode volume moving away from the fiber taper (bottom).

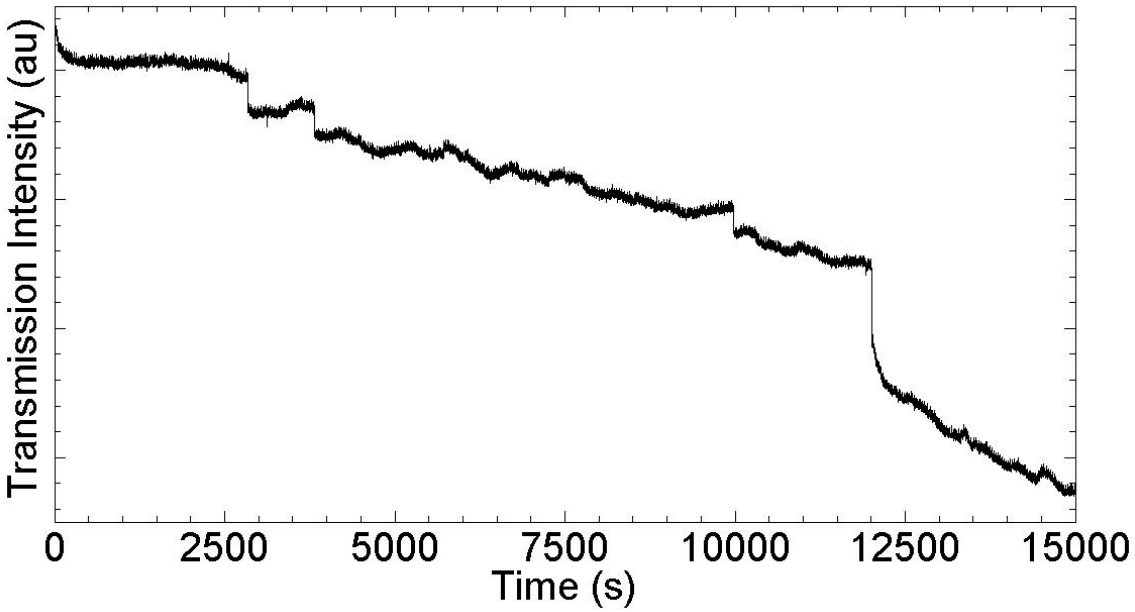

Figure 2.6: Transmission of the light through the fiber taper as Au nanorods are only detected from discrete drops in the intensity due to binding.

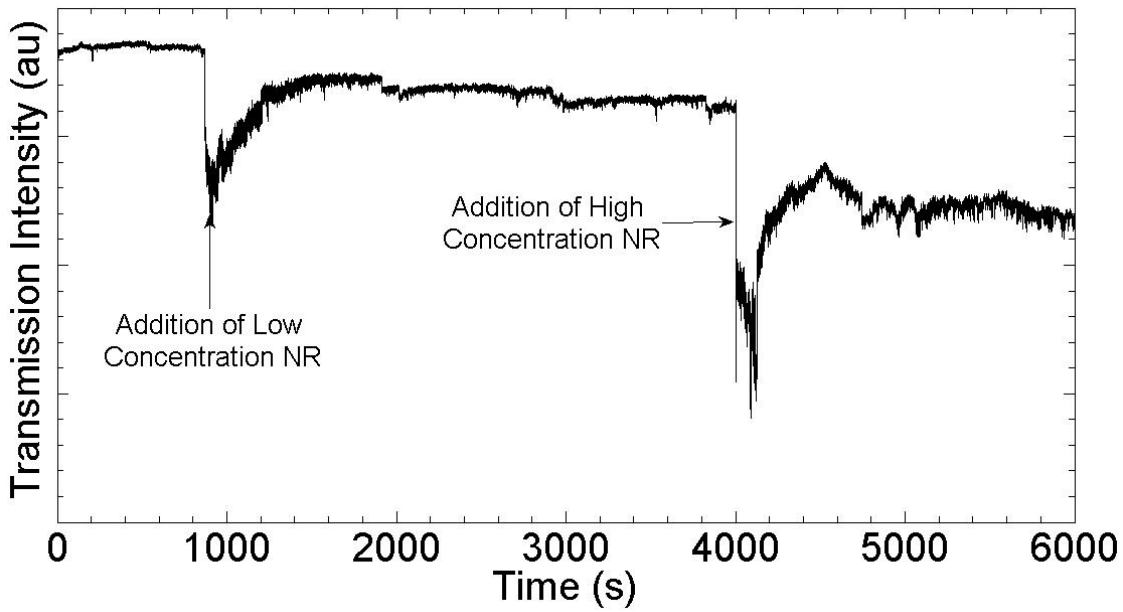

Figure 2.7: Transmission of the light through the fiber taper as LSPR of Au nanorods are excited and two different concentrations of the nanorods are detected. With increasing concentration the number of temporary dips also increase.

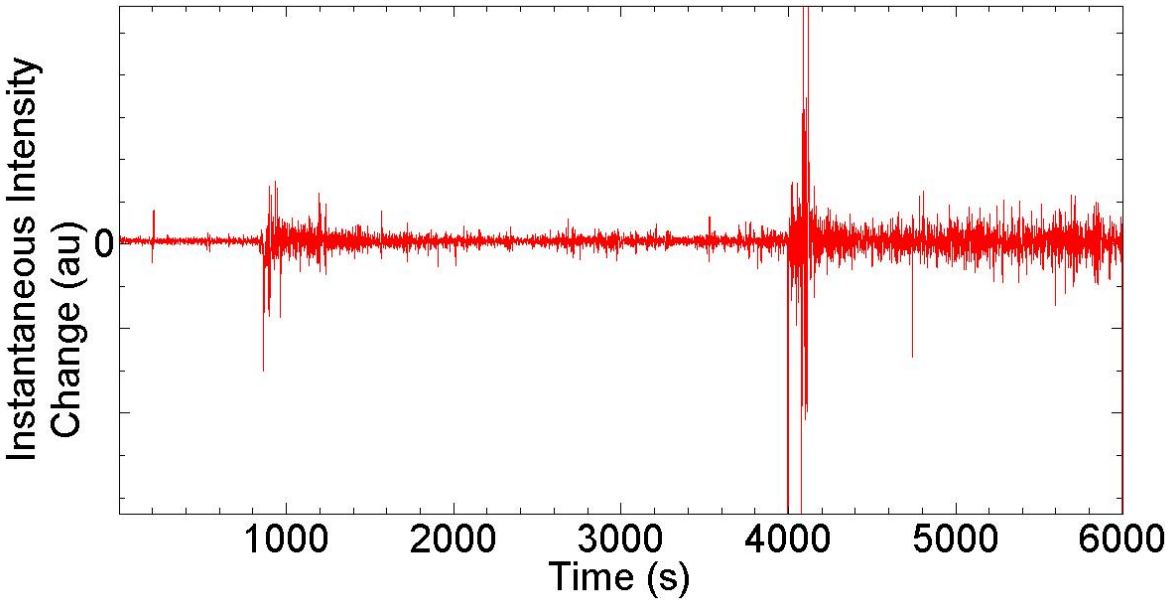

Figure 2.8: Instantaneous intensity drop obtained using a step function.

Chapter 3

Active Microtoroid Resonator Applications

3.1 Bidirectional Emission of Raman Laser

As mentioned in earlier chapters ultimate detection performance of microtoroid optical cavities are limited by the material absorption (silica, a low loss material for telecommunications band). In order to enhance the sensitivity, gain materials such as rare-earth ions are doped into silica microtoroids during fabrication [14]. Another way of inducing gain to reduce the losses due to material loss is to make use of the Raman gain in silica. Then, it is possible to push the limit of silica microtoroids further in detecting nanoparticles using mode splitting phenomena. For the detection of single nanoparticles with Raman gain assisted loss compensation and Raman laser it is of importance to show that Raman laser is bidirectional, that is when excited it exists in both clockwise and counterclockwise directions without the help of a scatterer.

In this experiment a microtoroid with no observable initial mode splitting was used. Raman laser was observed in both clockwise (CW) and counterclockwise (CCW) directions. When pumped at 1450 nm silica Raman gain generates Raman laser at around 1550 nm. Using a circulator and a wavelength division multiplexer, it is confirmed that when pumped at 1450 nm silica microtoroid exhibits no mode splitting therefore transmission of 1450 nm in the opposite direction to the input light was not existent (Figure 3.1a). Even though the input was unidirectional, Raman laser was observed in both CW (forward) and CCW

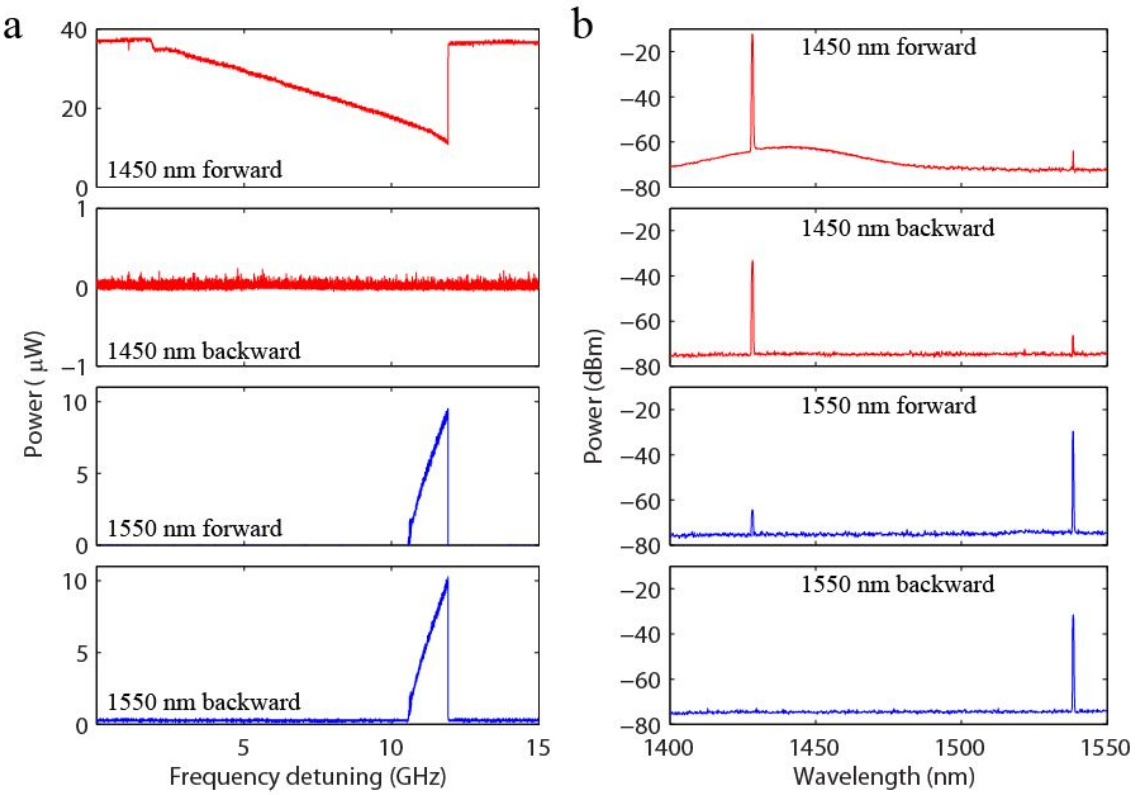

Figure 3.1: Experimental results showing the bidirectionality of Raman emission.(a)Transmission spectra and (b) optical spectrum obtained in the forward and backward directions for the pump laser in 1450 nm and the Raman emission in the 1550 nm band as the wavelength of the pump laser was scanned.

(backward) directions. Furthermore, optical spectrum analyzer measurements also confirmed the bi-directional emission of Raman laser (Figure 3.1b).

3.2 Blue Upconversion in Thulium Doped Silica Microcavities

Upconversion emission from rare-earth ion doped silica microcavities have been shown in green and infrared in the past [31]. However, infrared to blue upconversion have only been recently reported in silica microtoroids [18]. In this section, thulium doped microcavities exhibit blue upconversion using two different pumps: 660 nm and 980 nm. Even though the pump wavelengths are slightly offset from the ground state absorption of 690 nm and 1047 nm strong emission of blue light have been observed from silica microtoroids and microspheres.

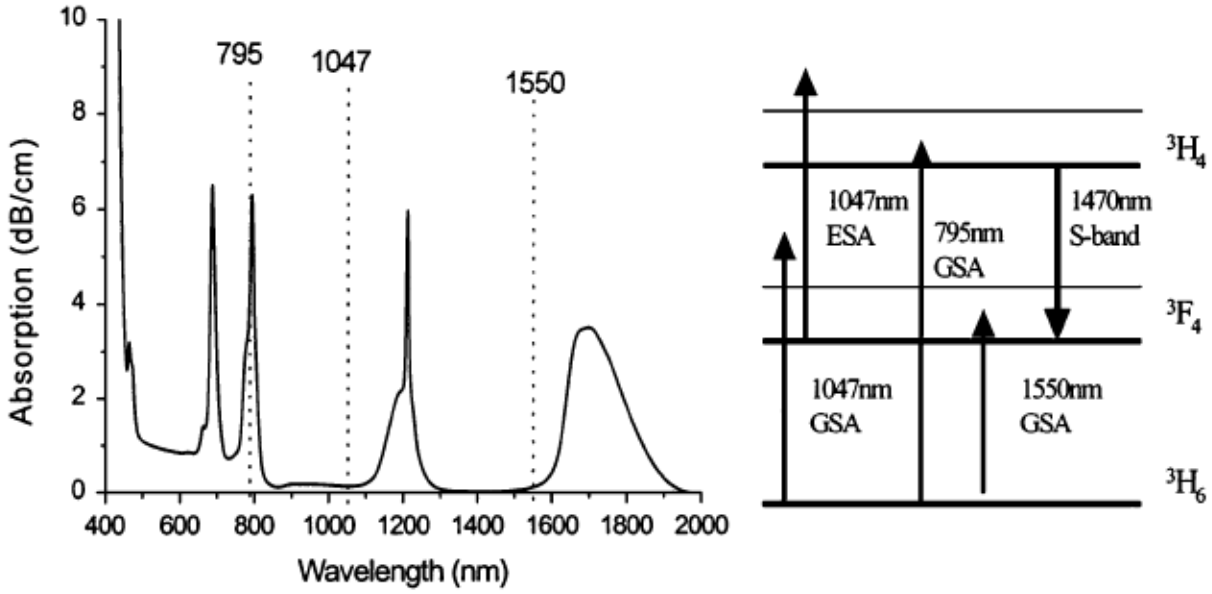

Figure 3.2: Energy level diagram (left) and ground state absorption spectrum (right) of Thulium [24].

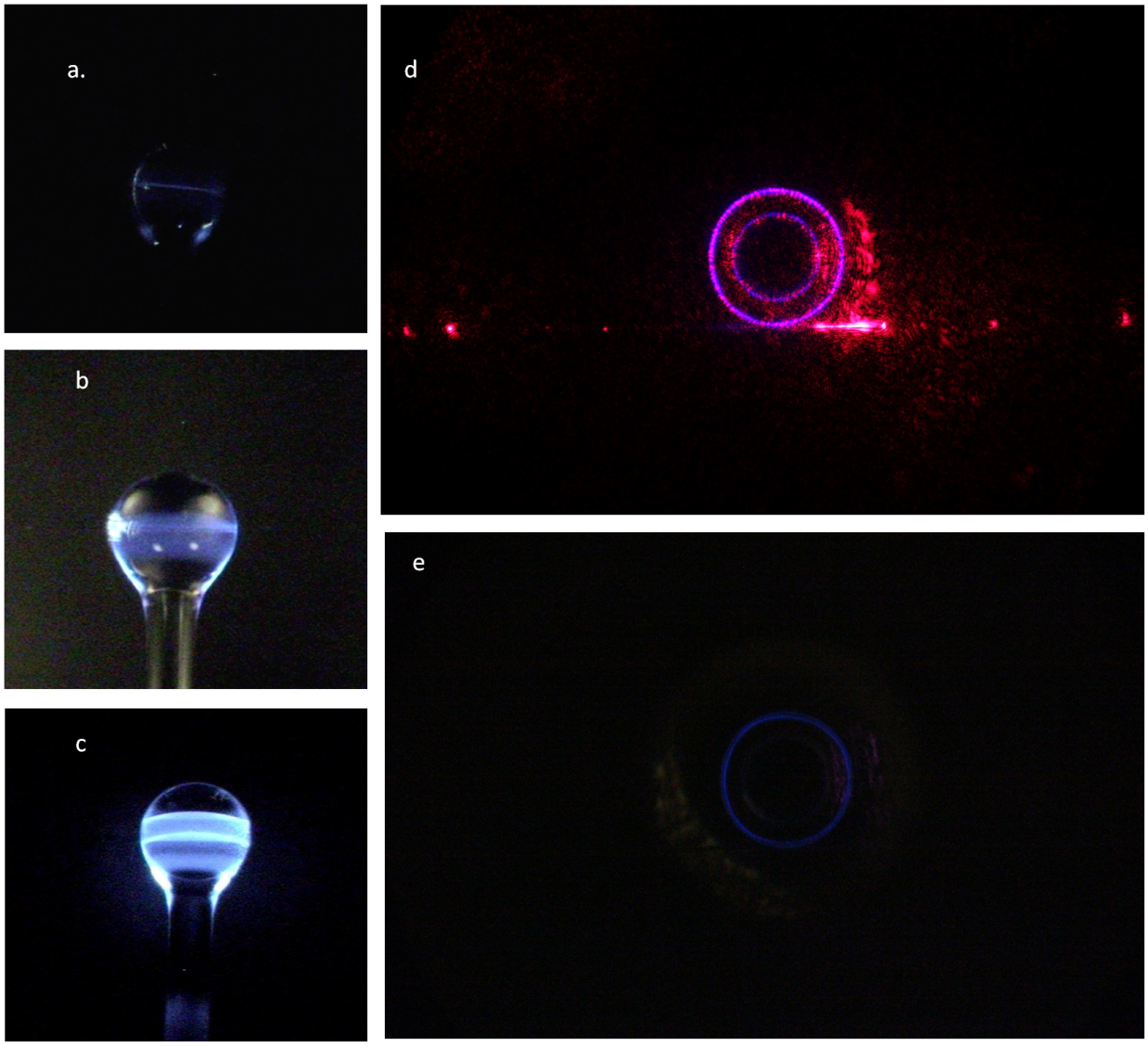

Figure 3.3: Optical microscope images of Thulium doped microcavities. **a, b** and **c** shows emission of blue light from silica microspheres doped with different concentrations of Thulium ions. As the ion concentration increases the location of the mode gets clear. **d** is emission of blue light from a Thulium doped microtoroid with 980 *pump*. **e** is emission due to pumping at 660 *nm*.

Appendix A

Optical Resonances of Microspheres

In order to understand the characteristics of the optical resonances of microspheres, the electromagnetic problem has to be solved. The solutions to the Helmholtz Equation for spherical boundary conditions were obtained by Mie first in the 19th century. Attaining the solutions for the electromagnetic problem requires a rigorous derivation. In this thesis, only key equations will be highlighted for a brief introduction.
Let us consider a plane wave for the excitation of resonances. In this context, notations for spherical coordinates will be used. A plane wave can be expanded in terms of vector spherical harmonics. The characteristic equations that satisfy the scalar wave equation in spherical polar coordinates are then,

$$\psi_{emn} = \cos(m\phi) P_n^m(\cos\theta) z_n(kr) \tag{A.1}$$

$$\psi_{omn} = \sin(m\phi) P_n^m(\cos\theta) z_n(kr) \tag{A.2}$$

where P_n^m is the Legendre polynomials of the first kind of degree n and order m and $z_n(kr)$ represents the spherical Bessel functions. Hence the vector spherical harmonics expansion of a plane wave is,

$$\vec{E_l} = E_0 \sum_{i=1}^{\infty} i^n \frac{2n+1}{n(n+1)} (\vec{M}_{o1n}^{(1)} - i\vec{N}_{e1n}^{(1)}) \tag{A.3}$$

where $\vec{M}_{o1n}^{(1)} = \vec{\nabla} \times (\vec{r}\psi_{o1n})$ and $\vec{N}_{e1n}^{(1)} = \frac{\vec{\nabla}\times\vec{M}_{e1n}^{(1)}}{k}$) [12, 26]. For a homogeneous, isotropic microsphere with radius a, the scattered electric field is then expressed as

$$\vec{E}_l = \sum_{i=1}^{\infty} E_n(a_n i\vec{N}_{e1n}^{(3)} - b_n\vec{M}_{o1n}^{(3)}) \tag{A.4}$$

The elastic scattering coefficients, a_n and b_n, can be simplified by the help of the Riccati-Bessel functions,

$$\psi_n(r) = rj_n(r) \tag{A.5}$$

$$\xi(r) = rh_n^{(1)}(r) \tag{A.6}$$

where $j_n(r)$ and $h_n^{(1)}$ are the cylindrical Bessel function and the spherical Hankel function of the first kind. Finally a_n and b_n can be expressed as

$$a_n = \frac{\psi_n^{'}(nka)\psi_n(ka) - n\psi_n^{'}(ka)\psi_n(nka)}{\psi_n^{'}(nka)\xi_n(ka) - n\psi_n(nka)\xi_n^{'}(ka)} \tag{A.7}$$

$$b_n = \frac{n\psi_n^{'}(nka)\psi_n(ka) - \psi_n^{'}(ka)\psi_n(nka)}{n\psi_n^{'}(nka)\xi_n(ka) - \psi_n(nka)\xi_n^{'}(ka)} \tag{A.8}$$

where k is the propagation constant, a is the microsphere radius and n is the refractive index of the microsphere. Note that, equations A.6 and A.7 are obtained for plane wave excitation of optical resonances. However, for most of the applications guided waves are used hence the profile of the input light beam has to be introduced into the elastic scattering coefficients. Nevertheless, the denominators of the scattering coefficients will not change because the resonances occur at the poles and are defined with the parameter, ka and the refractive index, n [2, 4]. Moreover, there are two scattering coefficients which correspond to the two classes of solutions. One of which is for transverse electric (TE) modes because of the absence of electric field in the direction of propagation of the electromagnetic field in

the microsphere. Transverse magnetic (TM) modes are defined in the same sense. Along the microsphere circumference where the resonant field stands in, TM modes have electric field components. As a result, electric fields of TM modes posses a more radial character.

References

[1] Jeffrey N. Anker. Biosensing with plasmonic nanosensors. *Nature Materials*, 7:442–453, June 2008.

[2] C. F. Bohren. *Absorption and Scattering of Light by Small Particles*. Interscience, New York, 1983.

[3] Thomas P. Burg. Weighing of biomolecules, single cells and single nanoparticles in fluid. *Nature*, 446:1066–1069, April 2007.

[4] Richard Chang. *Optical Effects Associated with Small Particles*. World Scientific, Singapore, 1988.

[5] Brian Cunningham. Colorimetric resonant reaction as a direct biochemical assay technique. *Sensors and Actuators B: Chemical*, 81:316–328, January 2002.

[6] S. Demarche. Techniques for recording reconstituted ion channels. *Analyst*, 136:1077–1089, January 2011.

[7] X. D. Fan. Sensitive optical biosensors for unlabeled targets: A review,. *Anal. Chim. Acta*, 620:8–26, March 2008.

[8] M. L. Gorodetsky. Ultimate q of optical microsphere resonators. *Optics Letters*, 21:453–455, April 1996.

[9] J. B. Heng. Sizing dna using a nanometer-diameter pore. *Biophysical Journal*, 87:2905–2911, October 2004.

[10] Heather K. Hunt. Bioconjugation strategies for microtoroidal optical resonators. *Sensors*, 10:9317 – 9336, October 2010.

[11] Heather K. Hunt. Label-free biological and chemical sensors. *Nanoscale*, 2:1544–1559, May 2010.

[12] M Kerker. *The Scattering of Light and Other Electromagnetic Radiation*. Academic Press, New York, 1969.

[13] Woosung Kim. Observation and characterization of mode splitting in microsphere resonators in aquatic environment. *Applied Physics Letters*, 98:141106 – 141106, April 2011.

[14] Tau Lu. A narrow-linewidth on-chip toroid raman laser. *IEEE Journal of quantum electronics*, 47:320 – 326, March 2011.

[15] MS Luchansky. Sensitive on-chip detection of a protein biomarker in human serum and plasma over an extended dynamic range using silicon photonic microring resonators and sub-micron beads. *Lab Chip*, 11:2042 – 2044, June 2011.

[16] Sudeep Mandal. A multiplexed optofluidic biomolecular sensor for low mass detection. *Lab on a Chip*, 9:2924–2932, June 2009.

[17] Adam D. Mcfarland. Single silver nanoparticles as real-time optical sensors with zeptomolar sensitivity. *Nano Letters*, 3:1057–1062, July 2003.

[18] Simin Mehrabani. Blue upconversion laser based on thulium-doped silica microcavity. *Optics letters*, 38:4346 – 4349, November 2013.

[19] Fernando Patolsky. Electrical detection of single viruses. *PNAS*, 101:14017 – 14022, September 2004.

[20] Abraham J. Qavi. Label-free technologies for quantitative multiparameter biological analysis. *Anal Bioanal Chem.*, 394:121 – 135, May 2010.

[21] Laura Sagle. Advances in localized surface plasmon resonance spectroscopy biosensing. *Nanomedicine*, 6:1447 – 1462, October 2011.

[22] Mehmet Sarikaya. Molecular biomimetics: nanotechnology through biology. *Nature Materials*, 2:577 – 585, September 2003.

[23] C. Tamerler. Molecular biomimetics: Genetic synthesis, assembly, and formation of materials using peptides. *MRS Bulletin*, 33:504 – 512, May 2008.

[24] E.R.M. Taylor. Thulium-doped tellurite fiber amplifier. *IEEE photonics technology letters*, 16:777 – 779, March 2004.

[25] Turner, A.P.F. *Biosensors: Fundamentals and Applications*. Oxford University Press, Oxford, 1987.

[26] H. C. van de Hulst. *Light Scattering by Small Particles*. Dover, New York, 1981.

[27] Frank Vollmer. Protein detection by optical shift of a resonant microcavity. *Applied Physics Letters*, 80:4057 – 4060, May 2002.

[28] Frank Vollmer. Whispering-gallery-mode biosensing: label-free detection down to single molecules. *Nature Methods*, 5:591 – 596, June 2008.

[29] Jie Xu. Detection of avian influenza virus using an interferometric biosensor. *Anal Bioanal Chem*, 389:1193–1199, August 2007.

[30] Q. F. Xu. All-optical logic based on silicon micro-ring resonators. *Optics Express*, 15:924–929, February 2007.

[31] Lan Yang. Fiber-coupled erbium microlasers on a chip. *Applied Physics Letters*, 83:825 – 826, August 2003.

[32] Yariv, AmnonYeh,Pochi. *Photonics*. Oxford University Press, New York, 2007.

[33] Gengfeng Zheng. Multiplexed electrical detection of cancer markers with nanowire sensor arrays. *Nature Biotechnology*, 23:1294–1301, September 2005.

[34] Hongying Zhu. Phage-based label-free biomolecule detection in an opto-fluidic ring resonator. *Biosensors and Bioelectronics*, 24:461 – 466, November 2008.

[35] Jiangang Zhu. On-chip single nanoparticle detection and sizing by mode splitting in an ultrahigh-q microresonator. *Nature Photonics*, 4:46–49, December 2010.

[36] Jiangang Zhu. Optical detection of single nanoparticles with a sub-wavelength fiber-taper. *Photonics Technology Letters, IEEE*, 23:1346 – 1348, September 2012.

Vita

Huzeyfe Yilmaz

Degrees B.S. Physics, February 2009
M.S. Physics, August 2011
M.S. Electrical Engineering, August 2014

Professional Societies IEEE Photonics
SPIE Photonics

Publications Yilmaz Huzeyfe (2013), New Journal of Physics, *Statistics of multiple-scatterer-induced frequency splitting in whispering gallery microresonators and microlasers* **15**(073030).

Yilmaz, Huzeyfe (2014), Proceedings of the National Academy of Sciences, *Raman-gain induced loss-compensation in whispering-gallery-microresonators and single-nanoparticle detection with whispering-gallery Raman-microlasers*, **Under Revision**.

August 2014

Cavities and Fiber Tapers as Sensors , Yilmaz, M.S. 2014